

Location and thermal evolution of the pseudogap due to spin fluctuations

Mengxing Ye,^{1,2} Zhentao Wang,^{3,*} Rafael M Fernandes,³ and Andrey V Chubukov⁴

¹*Kavli Institute for Theoretical Physics, University of California, Santa Barbara, CA 93106, USA*

²*Department of Physics and Astronomy, University of Utah, Salt Lake City, UT 84112, USA*

³*School of Physics and Astronomy, University of Minnesota, Minneapolis, MN 55455, USA*

⁴*School of Physics and Astronomy and William I. Fine Theoretical Physics Institute, University of Minnesota, Minneapolis, MN 55455, USA*

(Dated: April 19, 2023)

We study pseudogap behavior in a metal near a spin density wave (SDW) instability due to thermal magnetic fluctuations. We consider the $t-t'$ Hubbard model on a square lattice at a finite doping, at intermediate coupling strength, and analyze the thermal evolution of the electron spectral function between a SDW ordered state at low temperatures and a normal Fermi liquid at high temperatures. We argue that for proper description of the pseudogap one needs to sum up infinite series of diagrams for both the fermionic self-energy and the SDW order parameter in the SDW state or the magnetic correlation length in the paramagnetic state. We use eikonal approach to sum up an infinite series of diagrammatic contributions from thermal fluctuations. Earlier studies found that in the SDW state, the spectral function $A_{\mathbf{k}}(\omega)$ of a hot fermion at a finite T is exponentially small below the energy scale $\Delta(T)$, which scales with SDW order and vanishes at the ordering temperature T_N , and has a hump at a larger frequency Δ_{pg} , comparable to the zero-temperature SDW gap $\Delta(T=0)$. We argue that the hump, which we associate with the pseudogap, survives in some T range above T_N . We show that this range is split by regions of strong and weak pseudogap behavior. In the first region, Δ_{pg} is weakly temperature dependent, despite that it comes from thermal fluctuations. Such a behavior has been seen in numerical studies of the Hubbard model. We show that to obtain it, one needs to go beyond the one-loop approximation and sum up the infinite series of diagrams. In the second regime, Δ_{pg} decreases with increasing T and eventually vanishes. We further argue that a magnetic pseudogap at a finite T emerges only if the ground state is magnetically ordered. We present the phase diagram and apply the results to high- T_c cuprates.

I. INTRODUCTION

The origin of the pseudogap behavior, observed in the cuprates and other correlated materials, is still a subject of ongoing debates. Theoretical proposals for the pseudogap can be broadly split into three categories. One set of proposals is that the pseudogap phase is a new state of matter with some particle-hole order. The order can be either a conventional one, like spin-density wave (SDW) or charge-density wave (CDW) [1–4], or less conventional, like a circulating current [5, 6]. The second type of proposals is that the pseudogap phase is a state with a topological order, whose feedback effect on fermions mimics that of a SDW order [7–11]. Finally, the third set of proposals is that pseudogap is not an ordered state, but rather a precursor to either a superconductor [12–16] or a SDW order [17–21].

This paper is devoted to the analysis of the third scenario, more specifically to precursors to (π, π) antiferromagnetic order in 2D. The generic motivation here is based on neutron scattering, x-ray, and other measure-

ments, which show that, e.g., in the cuprates, magnetic fluctuations remain strong in the paramagnetic phase in a sizable range of dopings and temperatures, which includes the pseudogap region (see e.g. [22, 23] and references therein). We note in passing that the pairing interaction, mediated by soft overdamped spin fluctuations, is attractive in the d -wave channel; as such, a spin-fluctuation scenario for pairing has been widely discussed for cuprates and other materials [24].

In simple words, a precursor behavior to the SDW means the following: In the SDW ordered state the Fermi surface gets reconstructed due to doubling of the unit cell, and a gap $\Delta(T)$ opens up for “hot” fermions, whose Fermi momenta \mathbf{k}_{hs} (see Fig. 1 a) are connected by the SDW wave-vector $\mathbf{Q} \approx (\pi, \pi)$. The spectral function $A_{\mathbf{k}_{hs}}(\omega)$ for such fermions has two δ -function peaks at $\omega + \delta\mu \approx \pm\Delta$, where $\delta\mu = \mu - \mu_0$, and μ and μ_0 are the actual chemical potential and the one for free fermions. A precursor to a SDW is a state above T_N , in which the spectral function is continuous and non-zero for all ω , yet there are maxima (humps) at energies $\omega + \delta\mu \approx \pm\Delta_{\text{pg}}$, where over some range of $T > T_N$, Δ_{pg} is comparable to $\Delta(T=0)$ (see Fig. 1). A convention, widely used in the interpretation of photoemission results, is that pseudogap behavior holds when the spectral function of a hot

* Present address: Center for Correlated Matter and School of Physics, Zhejiang University, Hangzhou 310058, China

fermion has two peaks at a finite frequency, and a normal metallic behavior holds when it has a single peak at zero frequency.

We emphasize that precursor behavior is different from a non-Fermi liquid behavior caused by coupling to soft overdamped spin fluctuations. The latter gives rise to strong frequency dependent self-energy, which distributes the spectral weight over a wide range of frequencies. Yet, the maximum of $A_{\mathbf{k}_{hs}}(\omega)$ remains at $\omega = 0$.

To see how both non-Fermi liquid and precursor behavior emerge within the spin-fluctuation scenario, consider a hot fermion, whose energy $\epsilon_{\mathbf{k}_{hs}} = \epsilon_{\mathbf{k}_{hs}+\mathbf{Q}} = \mu_0$, and analyze the one-loop self-energy due to spin fluctuation exchange [25]. On the Matsubara axis, $\Sigma(\mathbf{k}_{hs}, \omega_n) = \int d\Omega_m d\mathbf{q} G(\mathbf{k}_{hs} + \mathbf{q}, \omega_n + \Omega_m) \chi(\mathbf{q}, \Omega_m)$, up to a numerical factor, where G and χ are fermionic and spin-fluctuation propagators, respectively (we define Σ via $G^{-1} = G_0^{-1} - \Sigma$).

In a SDW state, $\chi(\mathbf{q}, \Omega)$ contains the δ -function piece $\Delta^2 \delta(\Omega_m) \delta(\mathbf{q} - \mathbf{Q})$, and the self-energy is $\Sigma(\mathbf{k}_{hs}, \omega_n) = \Delta^2 G(\mathbf{k}_{hs} + \mathbf{Q}, \omega_n) \approx \Delta^2 / (i\omega_n - (\epsilon_{\mathbf{k}_{hs}+\mathbf{Q}} - \mu)) = \Delta^2 / (i\omega_n + \delta\mu)$. On the real frequency axis, this self-energy has a pole at $\omega = -\delta\mu - i0$. Using $G^{-1}(\mathbf{k}_{hs}, \omega) = \omega + i0 + \delta\mu - \Delta^2 / (\omega + i0 + \delta\mu)$, one immediately finds that the spectral function $A_{\mathbf{k}_{hs}}(\omega)$ has two peaks at $\omega + \delta\mu = \pm\Delta$. A precursor to SDW in the paramagnetic state emerges when the self-energy still has a pole at a finite $\omega = -\delta\mu$, but the pole moves to the lower frequency half-plane due to finite damping.

At $T = 0$ this does not happen because dynamical spin fluctuations are Landau overdamped and are slow modes compared to fermions. In this situation, the leading term in the self-energy is the convolution of the local Green's function, integrated over the momentum component perpendicular to the Fermi surface, and local bosonic propagator, integrated over the momentum that connects two points on the Fermi surface. This self-energy $\Sigma(\mathbf{k}_{hs}, \omega_n) = \int d\Omega G_L(\omega_n + \Omega_m) \chi_L(\Omega_m)$ strongly depends on frequency and gives rise to a redistribution of the spectral weight away from $\omega = 0$, but it has no pole.

The situation changes at a finite T . Now integration over Ω_m is replaced by summation over $\Omega_m = 2\pi mT$, and the self-energy contains the thermal contribution from static SDW fluctuations. The corresponding self-energy is $\Sigma_{\text{th}} = T \int d\mathbf{q} G(\mathbf{k}_{hs} + \mathbf{q}, \omega) \chi(\mathbf{q}, 0)$. It is natural to assume that near a SDW instability, $\chi(\mathbf{q}, 0)$ has an Ornstein-Zernike form $\chi(\mathbf{q}, 0) \propto [(\mathbf{q} - \mathbf{Q})^2 + \xi^{-2}]^{-1}$, where ξ is the magnetic correlation length. The integral $\int d\mathbf{q} \chi(\mathbf{q}, 0)$ is then confined to small $\mathbf{q} - \mathbf{Q}$ in dimensions $d \leq 2$. To first approximation one can then replace $G(\mathbf{k}_{hs} + \mathbf{q}, \omega)$ by $G(\mathbf{k}_{hs} + \mathbf{Q}, \omega)$ and move it out of momentum integral. One then obtains the same

$\Sigma_{\text{th}} = \left(\Delta_{\text{pg}}^{(1)}\right)^2 / (\omega + i0 + \delta\mu)$ as in the SDW state, with $\left(\Delta_{\text{pg}}^{(1)}\right)^2 = T \int d\mathbf{q} \chi(\mathbf{q}, 0)$. This form is indeed an approximate one as replacing $G(\mathbf{k}_{hs} + \mathbf{q}, \omega)$ by $G(\mathbf{k}_{hs} + \mathbf{Q}, \omega)$ and moving it out from the momentum integral is only approximately correct when $\chi(\mathbf{q}, 0)$ is not a δ -function. In more accurate one-loop calculations [12, 26, 27] the pole in $\Sigma(\mathbf{k}_{hs}, \omega)$ moves to the lower half-plane or transforms into a branch cut of the complex frequency. This gives rise to broadening of the peak in the spectral function, yet the maximum at $\omega + \delta\mu = \pm\Delta_{\text{pg}}^{(1)}$, survives in a finite T range. For $d = 2$, which we consider below, $\int d\mathbf{q} \chi(\mathbf{q}, 0) \propto \log \xi$, and $\Delta_{\text{pg}}^{(1)} \sim \sqrt{T \log \xi}$.

Pseudogap behavior at a finite T in 2D has been extensively studied numerically in the last few years [28–32], using various modern computational techniques for the Hubbard model, and was clearly detected at half-filling. The fluctuation diagnostics method identified static antiferromagnetic fluctuation as the source of the pseudogap behavior [29]. An identification of the pseudogap scale with the one-loop $\Delta_{\text{pg}}^{(1)}$ is a more subtle issue. Δ_{pg} , extracted from the numerical data, depends only weakly on temperature in a finite temperature window above T_N (Ref. [32]), while $\Delta_{\text{pg}}^{(1)} \sim T \log \xi$ contains T as an overall scale. The authors of [32] argued that their data for the magnetic correlation length are consistent with the exponential behavior $\xi \propto e^{T_0/T}$. Then $\log \xi \sim 1/T$ compensates the overall T , and $\Delta_{\text{pg}}^{(1)}$ becomes T -independent, like the measured Δ_{pg} . However, the exponential temperature dependence of ξ holds in a 2D Heisenberg model for localized spins [33], but there is no obvious reason why it should hold in a metal. Indeed, using the one-loop approximation for the spin susceptibility, one obtains that ξ only weakly depends on T , hence $\Delta_{\text{pg}}^{(1)}$ scales roughly as T , in disagreement with the numerical data.

Another issue is the location of the pseudogap phase. At a first glance, it should exist at a finite T as long as spin correlation length is large, even if the ground state is not magnetically ordered. However, extensive quantum Monte-Carlo studies of fermion-boson models with a paramagnetic ground state found no evidence for the pseudogap [34, 35]. Recent numerical studies of the Hubbard model at a finite doping also argued that pseudogap phase at a finite T exists only in the range of dopings where the ground state possesses some magnetic order [36].

The goal of this work is to resolve these issues. For this we adopt the computational technique known as eikonal approach, which allows one to sum up thermal contributions to the fermionic Green's function up to an infinite order. This technique has been applied to analyze how the pseudogap survives when long-range magnetic

order gets destroyed by thermal fluctuations [20, 21], and how thermal fluctuations lead to pseudogap formation when one departs from a metal [17–19]. These last studies, however, used the magnetic correlation length ξ as an input parameter. Below we extend the eikonal approach to spin polarization in the paramagnetic phase, from which we extract the temperature dependent correlation length $\xi(T)$. We show that the pseudogap behavior does develop above T_N , and the pseudogap scale Δ_{pg} , extracted from the full Green’s function, is comparable to the $\Delta_{\text{pg}}^{(1)} \propto (T \log \xi)^{1/2}$, where $\xi = \xi(T)$ is the fully dressed correlation length. In a sizable range of T above T_N , this $\xi(T)$ is, to a good accuracy, exponential in $1/T$, such that Δ_{pg} is nearly independent on T . This is consistent with Ref. [32]. We further show that when the ground state is non magnetically ordered, the pseudogap does not develop due to non-exponential, but still strong temperature variation of the full $\xi(T)$, which keeps the system in a weak coupling regime.

A. Summary of the results

We study thermal evolution of the spectral function in the Hubbard model with hopping t between nearest and t' between next-nearest neighbors, by varying T and U at a given hole doping $x > 0$. At large U , the relevant energy scale for magnetic fluctuations is $J = 4t^2/U$. Like we said, we focus on “hot” fermions, for which $\epsilon_{\mathbf{k}} \approx \epsilon_{\mathbf{k}+\mathbf{Q}} \approx \mu_0$.

Thermal fluctuations in the magnetically-ordered state at $T < T_N$ have been analyzed before, and we use these earlier results as input for our studies [20, 21]. The strength of thermal fluctuations is controlled by the dimensionless parameter $\mathfrak{t}^* = \frac{T}{J} |\log \epsilon| \propto \frac{T}{T_N}$, where ϵ is a deviation from two-dimensionality (the parameter that cuts 2D logarithms at infinite ξ). Deep in the ordered phase at $T \ll T_N$, the spectral function of a fermion at a hot spot nearly vanishes below the scale set by the true SDW order $\Delta(T)$, and is peaked at $\omega + \delta\mu = \pm\Delta(T)$. (Fig. 1(b)). In this regime, $\delta\mu$ is negative and is comparable by magnitude to $\Delta(T)$. For such low T , the one-loop mean field approximation works well. As T increases, the SDW order parameter $\Delta(T)$ shrinks, and the spectral function displays two features: (i) a true gap below $\Delta(T)$ (up to $e^{-\Delta(T)/T}$ corrections), and (ii) a hump at $\omega + \delta\mu = \pm\Delta_{\text{pg}}(T) > \Delta(T)$, where $\Delta_{\text{pg}}(T) \sim U\sqrt{\mathfrak{t}^*} \sim U$ near T_N . The chemical potential is located between the SDW gap $\Delta(T)$ and the hump energy $\Delta_{\text{pg}}(T)$ (see Fig. 1(c)). In the extreme case of U much larger than the bandwidth, $\Delta_{\text{pg}} \approx U/2$ and $\delta\mu \approx \mu \approx -U/2$, with corrections of order J . The humps are then located at $\omega \approx U$ and at $\omega \sim -J$. At $T = T_N$, $\Delta(T)$ vanishes

and the spectral function becomes non-zero at all finite frequencies. Yet, the spectral function still has peaks at $\omega + \delta\mu = \pm\Delta_{\text{pg}}$.

The key result of our analysis is the identification of the system behavior in the paramagnetic phase. We argue that the strength of the thermal contribution to the self-energy is determined by the dimensionless coupling $\lambda = \lambda(T) \propto T\xi^2(T)$. A pseudogap behavior develops when λ is larger than critical $\lambda_c = O(1)$. This definitely holds above T_N , where $\xi(T)$ diverges.

We argue that the proper description of thermal fluctuations at large λ requires one to sum up infinite series of diagrams for the fermionic self-energy *and* for the polarization bubble, from which we extract the fully dressed correlation length $\xi(T)$. The series can be viewed perturbatively as an expansion in $\mathfrak{t}_0 \sim \frac{T}{J} |\log \xi_0|$, where ξ_0 is the bare magnetic correlation length. In our calculations, we re-express the series in terms of $\mathfrak{t} \sim \frac{T}{J} |\log \xi|$, where ξ is the actual, fully renormalized correlation length, which we compute self-consistently. We explicitly sum up the series by converting them into certain integrals, which we evaluate analytically and obtain exact analytical formulas for the fully dressed fermionic Green’s function and the correlation length. We find that the dressed ξ is exponential in T_0/T , where $T_0 \sim J$. The parameter $\mathfrak{t} \sim (T/J) \log \xi$ is then $O(1)$, which in turn justifies the need to sum up infinite series of thermal contributions to the self-energy and the polarization bubble. The fully dressed pseudogap scale, defined as $\Delta_{\text{pg}}^{(e)}$, scales as $(T \log \xi)^{1/2}$, like the one-loop pseudogap, and is almost independent on T . Its magnitude is the same as $\Delta_{\text{pg}}^{(e)}$ in the SDW state near T_N . These results are in agreement with the numerical data [32]. We show the spectral function in this regime in Fig. 1(d). It was termed a “strong pseudogap regime”, based on the analysis of the experimental data from various probes [17, 37]

For smaller λ , but still larger than the critical one, the self-energy due to thermal fluctuations changes because one cannot pull fermionic Green’s function out of the momentum integral. This in turn changes the behavior of the correlation length, which is no longer exponential in $1/T$. We argue that $\lambda(T)$ decreases with increasing T , and the pseudogap energy also decreases and eventually vanishes at $T = T_p$ (Fig. 2). This regime was termed a “weak pseudogap regime” [17, 37]. The shrinking and eventual vanishing of Δ_{pg} is adequately described within the one-loop approximation. We also argue that quantum spin fluctuations (the ones with non-zero bosonic Matsubara frequencies) become comparable to thermal ones starting from $T_q \sim T_p$, i.e., to a reasonable approximation the end point of the pseudogap behavior is also the boundary between thermal and quantum regimes. At $T > T_p$, the system displays a conventional metallic be-

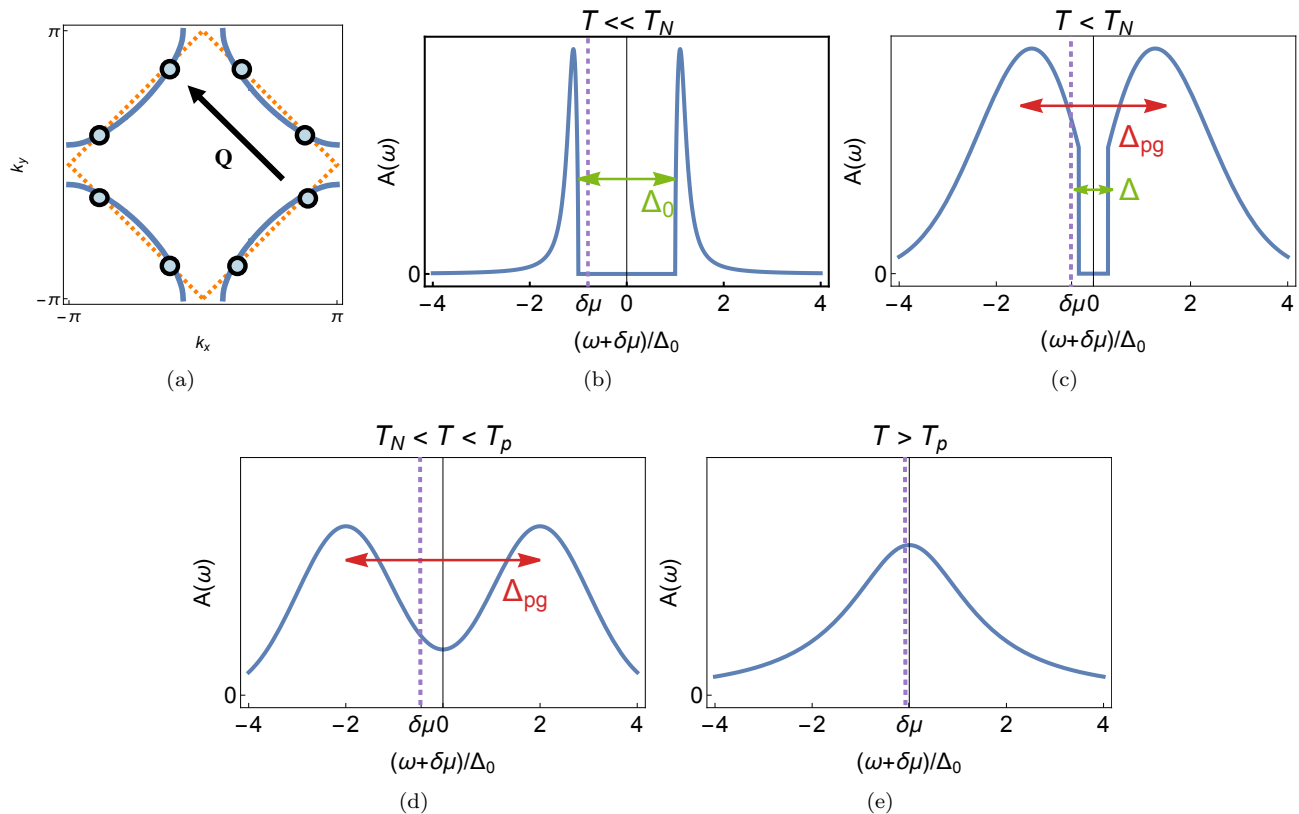


FIG. 1. (a) Fermi surface of the $t - t'$ model on a square lattice. The eight blue spots indicate the “hot spots” that satisfy $\epsilon_{\mathbf{k}} = \epsilon_{\mathbf{k}+\mathbf{Q}}$, where $\mathbf{Q} = (\pi, \pi)$. The orange dashed line specifies the folded Brillouin zone in the presence of (π, π) order. (b)-(e): Schematic plots of the electron spectral function at the hot spot (b) in the SDW state for $T \ll T_N$, (c) in the SDW state at T close to T_N , (d) in the pseudogap metal state, (e) in the normal Fermi liquid state. $\Delta_0 \approx U/2$ in panel (b) is the mean field SDW order parameter at $T = 0$. The quantity $\delta\mu = \mu - \mu_0$ is the difference between the actual chemical potential μ and the chemical potential for free fermions μ_0 . The purple dashed line indicates the position of the chemical potential.

havior, Fig. 1(e).

Right above a QCP, we find that $\xi^{-2}(T)$ scales as T , modulo logarithms. The coupling λ is then independent on T . We find that its value is below the critical λ_c , hence pseudogap behavior does not emerge. The same holds when ξ is finite at $T = 0$. Our results then show that pseudogap behavior emerges only when the ground state is magnetically ordered (Fig. 15). This agrees with recent numerical study of the Hubbard model [36] and with quantum Monte Carlo analysis of a fermion-boson model near a (π, π) SDW instability [38].

We apply the results to the cuprates and show the location of the pseudogap region due to thermal SDW fluctuations in Fig. 16. Most experiments indicate that in hole-doped cuprates a magnetic order is lost well before optimal doping. Our results indicate that in this situation, the observed pseudogap behavior below $T^*(x)$ in these materials is not due to thermal magnetic fluctuations and is either the result of strong pairing fluctuations [12–16], or reflects a hidden, possibly topological order below T^* [5–11] (Fig. 16 a). If, however, a

magnetic order (not necessary a (π, π) one) survives up to optimal doping, pseudogap behavior due to thermal magnetic fluctuations extends over a much wider range, and T_p , up to which this order holds, may be close to T^* (Fig. 16 b). This last behavior holds in electron-doped cuprates, where a SDW order extends almost up to optimal doping [23].

The paper is organized as follows. In Sec. II we introduce the model and review the mean field solution for the magnetically ordered state. Here we list the results for the dynamical magnetic susceptibility, the Goldstone modes, and the magnon-fermion vertex function. In Sec. III we discuss the procedure to study the pseudogap behavior from *static thermal fluctuations*. We first review the one-loop results both in the SDW-ordered phase and in the paramagnetic phase, and then discuss the eikonal approach, again first in the SDW phase and then in the paramagnetic phase, where we also discuss infinite series for the spin polarization bubble, from which we extract the temperature dependence of the correlation length. In Sec. IV we present our numerical solutions of

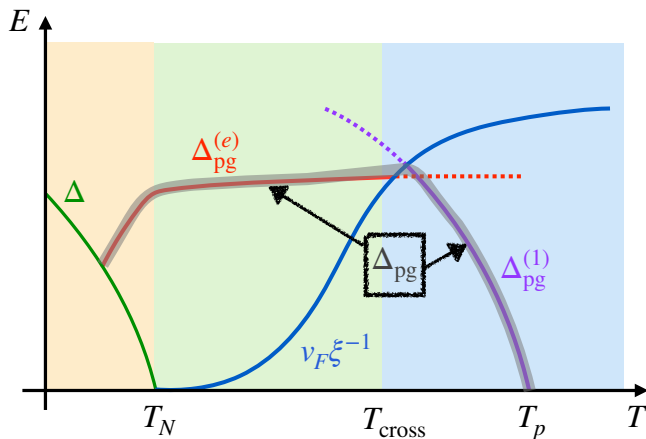


FIG. 2. Energy scales that determine the evolution of the spectral function with temperature: the SDW order parameter Δ (green line), the pseudogap energy from eikonal series $\Delta_{\text{pg}}^{(e)}$ (red line), the characteristic fermion energy $v_F \xi^{-1}$ (blue line) and the pseudogap energy from the one-loop calculation $\Delta_{\text{pg}}^{(1)}$ (purple line). The energy evolution of the pseudogap scale Δ_{pg} over the whole temperature range is highlighted in grey. The pseudogap emerges below T_N , remains almost a constant up to T_{cross} , and then decreases and eventually vanishes at T_p . The regions below and above T_{cross} are termed “strong” and “weak” pseudogap regimes. Note that quantum fluctuations become relevant at roughly the same T_p , where the pseudogap disappears (see Sec. IA for the detailed discussion).

eikonal equations for $\Delta(T)$, $\Delta_{\text{pg}}^{(e)}(T)$, and $v_F \xi^{-1}$ and analyze the evolution of the fermion spectral function. In Sec. IV A we locate the region, in which thermal fluctuations dominate, on the phase diagram of the spin-fermion model on the (T, x) plane, and compare our phase diagram with the experimental one for high- T_c cuprates. In Sec. V we summarize our findings.

II. THE MODEL

The point of departure for our analysis is the one band Hubbard model for spin 1/2 fermions on a square lattice with nearest and next-nearest neighbor hopping t, t' ,

$$\mathcal{H}_{\text{Hubbard}} = \sum_{\mathbf{k}} \sum_{\sigma} \epsilon_{\mathbf{k}} a_{\mathbf{k},\sigma}^{\dagger} a_{\mathbf{k},\sigma} + U \sum_i n_{i,\uparrow} n_{i,\downarrow}, \quad (1)$$

where $\epsilon_{\mathbf{k}} = -2t(\cos k_x + \cos k_y) - 4t' \cos k_x \cos k_y$. For numerical calculations we set $t = 0.3eV$ and $t' = -0.06eV$.

At small enough U , the ground state of $\mathcal{H}_{\text{Hubbard}}$ is a Fermi liquid with a Fermi surface whose size is related to electron density $1-x$ by Luttinger theorem. We show the Fermi surface of non-interacting fermions in Fig. 1 (a). Near half-filling (at small x), the Fermi surface contains 8 special points called hot spots, for which \mathbf{k} and $\mathbf{k} + \mathbf{Q} =$

$\mathbf{k} + (\pi, \pi)$, are both on the Fermi surface ($\epsilon_{\mathbf{k}} = \epsilon_{\mathbf{k}+\mathbf{Q}} = \mu_0$). For free fermions, the spectral function $A_{\mathbf{k}}(\omega)$ at a hot spot is a δ -function $\delta(\omega)$. At finite T and U , the δ -function broadens due to the fermionic self-energy, but remains peaked at $\omega = 0$ (panel (e) in Fig. 1).

We assume that at larger $U > U_c$, the ground state at half-filling is a SDW state with ordering wave vector \mathbf{Q} . The value of U_c is determined by solving the mean field equation for the SDW order parameter (See Fig. 13 for the solution of U_c at different dopings). We further assume that the parameters are such that a commensurate SDW order holds at a finite doping x , up to a critical $x_c(U)$. We do not consider here an incommensurate spin order at a finite x , and stripe configurations, which emerge when an incommensurate order melts down [39–43]. We describe the ground state and the finite temperature state proximate to the SDW by studying the mean field Hamiltonian and low energy fluctuations on top of it. In the strong coupling limit $U/t \gg 1$, this corresponds to the renormalized classical regime of the non-linear sigma model [44]. Our main interest here is to study the physics in the intermediate coupling regime, when the Hubbard U and the bandwidth are comparable.

We first review the mean field Hamiltonian, the low energy magnon dispersion, and the magnon-fermion coupling [45].

The mean field Hamiltonian reads

$$\mathcal{H}_{\text{MF}} = \sum_{\mathbf{k}}' \sum_{\sigma} \begin{pmatrix} a_{\mathbf{k},\sigma}^{\dagger} & a_{\mathbf{k}+\mathbf{Q},\sigma}^{\dagger} \end{pmatrix} \begin{pmatrix} \epsilon_{\mathbf{k}} & -\Delta_0 \text{sgn } \sigma \\ -\Delta_0 \text{sgn } \sigma & \epsilon_{\mathbf{k}+\mathbf{Q}} \end{pmatrix} \begin{pmatrix} a_{\mathbf{k},\sigma} \\ a_{\mathbf{k}+\mathbf{Q},\sigma} \end{pmatrix} \quad (2)$$

where $\Delta_0 = \frac{U}{2} \langle \sum_{\mathbf{k}} a_{\mathbf{k}+\mathbf{Q}}^{\dagger} \sigma_z a_{\mathbf{k}} \rangle$ is the SDW order parameter, $\sum_{\mathbf{k}}$ and $\sum_{\mathbf{k}}'$ denote the summation over the full and folded Brillouin zone, respectively, see Fig. 1a.

The standard Bogoliubov transformation diagonalizes the mean field Hamiltonian to

$$\mathcal{H}_{\text{MF}} = \sum_{\mathbf{k}}' \epsilon_{\mathbf{k}}^v \gamma_{\mathbf{k},\sigma}^v \dagger \gamma_{\mathbf{k},\sigma}^v + \epsilon_{\mathbf{k}}^c \gamma_{\mathbf{k},\sigma}^c \dagger \gamma_{\mathbf{k},\sigma}^c, \quad (3)$$

where $\epsilon_{\mathbf{k}}^{c,v} = \epsilon_{\mathbf{k}}^{\pm} \pm E_{\mathbf{k}}$ with $\epsilon_{\mathbf{k}}^{\pm} = \frac{\epsilon_{\mathbf{k}} + \epsilon_{\mathbf{k}+\mathbf{Q}}}{2}$, $\epsilon_{\mathbf{k}}^{-} = \frac{\epsilon_{\mathbf{k}} - \epsilon_{\mathbf{k}+\mathbf{Q}}}{2}$ and $E_{\mathbf{k}} = \sqrt{\Delta_0^2 + (\epsilon_{\mathbf{k}}^{-})^2}$. The valence and conduction band operators $\gamma_{\mathbf{k},\sigma}^v$ and $\gamma_{\mathbf{k},\sigma}^c$ are related to the original $a_{\mathbf{k},\sigma}$ and $a_{\mathbf{k}+\mathbf{Q},\sigma}$ as

$$\begin{pmatrix} a_{\mathbf{k},\sigma} \\ a_{\mathbf{k}+\mathbf{Q},\sigma} \end{pmatrix} = \mathbf{V}_{\mathbf{k},\sigma} \begin{pmatrix} \gamma_{\mathbf{k},\sigma}^v \\ \gamma_{\mathbf{k},\sigma}^c \end{pmatrix}, \quad \mathbf{V}_{\mathbf{k},\sigma} = \begin{pmatrix} \mathbf{v}_{\mathbf{k}} & -\text{sgn}(\sigma) \mathbf{u}_{\mathbf{k}} \\ \text{sgn}(\sigma) \mathbf{u}_{\mathbf{k}} & \mathbf{v}_{\mathbf{k}} \end{pmatrix}, \quad (4)$$

$$\mathbf{v}_{\mathbf{k}} = \sqrt{\frac{1}{2}\left(1 - \frac{\varepsilon_{\mathbf{k}}^-}{E_{\mathbf{k}}}\right)}, \quad \mathbf{u}_{\mathbf{k}} = \sqrt{\frac{1}{2}\left(1 + \frac{\varepsilon_{\mathbf{k}}^-}{E_{\mathbf{k}}}\right)}.$$

The low energy fluctuations in the SDW state are the Goldstone modes. They can be obtained by computing the magnetic susceptibility [46, 47]. The propagators of

the magnon mode $e_{\mathbf{q}}$ are

$$\begin{aligned} \mathcal{D}^{+, (0)}(\mathbf{q}, \Omega_m) &= -\langle T_{\tau} e_{\mathbf{q}}(\tau) e_{\mathbf{q}}^{\dagger}(0) \rangle_{\Omega_m} = \frac{1}{i\Omega_m - \Omega_{\mathbf{q}}}, \\ \mathcal{D}^{-, (0)}(\mathbf{q}, \Omega_m) &= -\langle T_{\tau} e_{\mathbf{q}}^{\dagger}(\tau) e_{\mathbf{q}}(0) \rangle_{\Omega_m} = \frac{-1}{i\Omega_m + \Omega_{\mathbf{q}}} \end{aligned} \quad (5)$$

where $\langle \mathcal{O}(\tau) \rangle_{\Omega_m} = \int_0^{\beta} d\tau e^{i\Omega_m \tau} \langle \mathcal{O}(\tau) \rangle$. In the small t'/t limit, $\Omega_{\mathbf{q}} \approx 4JS \sqrt{1 - \gamma_{\mathbf{q}}^2}$, where $\gamma_{\mathbf{q}} = \frac{1}{2}(\cos q_x + \cos q_y)$ and $J = 4t^2/U$. The dispersion $\Omega_{\mathbf{q}}$ is gapless at $\mathbf{q} = (0, 0)$ and $\mathbf{q} = (\pi, \pi)$, corresponding to the two Goldstone modes of fluctuations transverse to the SDW order.

The electron-magnon coupling is

$$\mathcal{H}_{\text{el-mag}} = \frac{U}{\sqrt{N}} \sum_{\mathbf{k}, \mathbf{q}} \left[\eta_{\mathbf{q}} \left(e_{-\mathbf{q}}^{\dagger} + e_{\mathbf{q}} \right) a_{\mathbf{k}+\mathbf{q}, \sigma}^{\dagger} a_{\mathbf{k}, \sigma'} + \bar{\eta}_{\mathbf{q}} \left(e_{-\mathbf{q}}^{\dagger} - e_{\mathbf{q}} \right) a_{\mathbf{k}+\mathbf{q}, \sigma}^{\dagger} a_{\mathbf{k}+\mathbf{Q}, \sigma'} \text{sgn}(\sigma) \right] \delta_{\sigma, -\sigma'}, \quad (6)$$

where $\delta_{\sigma, -\sigma'}$ is present because magnons are transverse fluctuations (we set the SDW staggered magnetization along \mathbf{z}). The coherence factors are $\eta_{\mathbf{q}} =$

$\frac{1}{\sqrt{2}} \left(\frac{1-\gamma_{\mathbf{q}}}{1+\gamma_{\mathbf{q}}} \right)^{1/4}$, $\bar{\eta}_{\mathbf{q}} = \frac{1}{\sqrt{2}} \left(\frac{1+\gamma_{\mathbf{q}}}{1-\gamma_{\mathbf{q}}} \right)^{1/4}$. We see that the magnon-fermion coupling scales as $\sqrt{|\mathbf{q}|}$ at small \mathbf{q} and diverges as $1/\sqrt{|\mathbf{q}-\mathbf{Q}|}$ at \mathbf{q} near \mathbf{Q} . In terms of the conduction and valence fermions $\gamma^{c,v}$, this interaction is

$$\mathcal{H}_{\text{el-mag}} = \frac{U}{\sqrt{N}} \sum_{\mathbf{k}} \sum'_{\mathbf{q}} \left\{ \gamma_{\mathbf{k}\sigma}^{c\dagger} \gamma_{\mathbf{k}+\mathbf{q}, \sigma'}^v \left[(\eta_{\mathbf{q}} - \bar{\eta}_{\mathbf{q}}) e_{\mathbf{q}}^{\dagger} + (\eta_{\mathbf{q}} + \bar{\eta}_{\mathbf{q}}) e_{-\mathbf{q}} \right] + h.c. \right\} \delta_{\sigma, -\sigma'} + \dots \quad (7)$$

where dots stand for the terms that involve only conduction or only valence fermions. Because the corresponding interaction vertices are small in $|\mathbf{q}|$, we will not include these terms in our analysis.

This interaction is illustrated graphically in Fig. 3. We use a wavy line for magnon propagator, solid straight line for fermion propagator, a filled (empty) circle \bullet (\circ) for magnon-fermion vertex with outgoing spin-down (spin-up) fermion and incoming spin-up (spin-down) fermion.

III. PSEUDOGAP FROM QUASISTATIC SPIN FLUCTUATIONS

In this section, we discuss how “hot” fermions develop pseudogap behavior at a finite T in both SDW state and paramagnetic state, due to the singular self-energy contribution from thermal (static) spin fluctuations. We will

identify a framework to study the effects of thermal fluctuations to infinite order in perturbation theory. To set the stage for our analysis, in Sec. III A we first review and extend the one-loop calculation of the fermion self-energy from thermal fluctuations and rationalize the need to include higher loop contributions. In Sec. III C, we discuss the computational procedure that allows one to sum up infinite series of thermal contributions to the fermionic self-energy and the bosonic polarization. This will allow us to determine self-consistently the fermionic Green’s function, the chemical potential, the SDW order parameter, and the spin correlation length in the paramagnetic phase.

A. One-loop analysis

The effects of quasistatic spin fluctuations have been studied both in the SDW state [20, 21] and in the para-

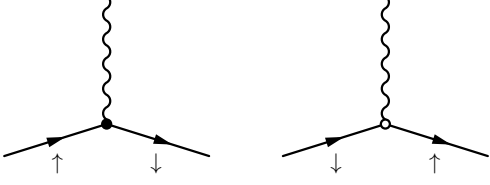


FIG. 3. Magnon-fermion vertex. The wavy line is used for magnon propagator, solid straight line for fermion propagator, a filled (empty) circle \bullet (\circ) for magnon-fermion vertex with outgoing spin-down (spin-up) fermion and incoming spin-up (spin-down) fermion. Note that in the SDW state, each vertex must connect one conduction fermion and one valence fermion.

magnetic state [17–19]. Here, we review and extend one-loop calculations in both phases and rationalize the need to include higher-loop contributions.

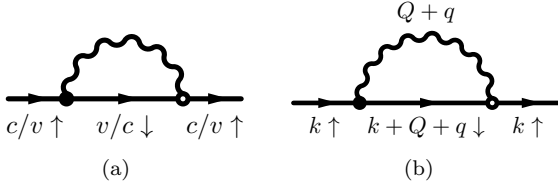


FIG. 4. One loop self-energy. (a) Leading order diagram (at $|\log \epsilon|$) in the SDW state. c, v denote the conduction and valence band fermions; \uparrow, \downarrow denote the spin up and spin down state. (b) Leading order diagram (at $|\log \xi|$) in the paramagnetic state from magnetic fluctuations in the transverse channel.

1. SDW state

For definiteness, consider the SDW ordered state at half-filling. The thermal one-loop correction to the SDW order parameter diverges logarithmically in 2D and immediately destroys long-range SDW order, in agreement with Mermin-Wagner theorem [48]. The one-loop fermionic self-energy is also logarithmically singular, but its effect is more nuanced, as we will see below. To circumvent the divergencies in 2D, we will consider the physics in dimension $2 + \epsilon$ and use $\epsilon \ll 1$ to regularize the logarithmic singularity. Physically, systems with small but finite ϵ are highly anisotropic 3D systems with small hopping along the z direction.

The one-loop correction to SDW order changes the order parameter Δ from $U/2$, which is its value at $T = 0$ and $U \gg t, t'$ to

$$\Delta = U \langle S_z \rangle = \frac{U}{2} (1 - \mathfrak{t}^*/2) \quad (8)$$

where

$$\mathfrak{t}^* = \frac{2T}{\pi JS} \ln \frac{\pi^2}{2\epsilon^2} \quad (9)$$

is a dimensionless parameter, which measures the strength of thermal fluctuations.

The one-loop self-energy for a conduction electron is given by the diagram in Fig. 4(a), using the magnon-fermion coupling vertex in Eq. (7). In analytical form,

$$\begin{aligned} \Sigma^{c(1)}(\mathbf{k}, i\omega_n) &= -U^2 \frac{T}{N} \sum_{\mathbf{q}, m} G^{v(0)}(\mathbf{k} + \mathbf{q}, i\omega_n + i\Omega_m) \left((\eta_{\mathbf{q}} - \bar{\eta}_{\mathbf{q}})^2 \mathcal{D}^{-(0)}(\mathbf{q}, i\Omega_m) + (\eta_{\mathbf{q}} + \bar{\eta}_{\mathbf{q}})^2 \mathcal{D}^{+(0)}(-\mathbf{q}, i\Omega_m) \right) \\ &\stackrel{\Omega_m=0}{=} -U^2 \frac{T}{N} \sum_{\mathbf{q}} G^{v(0)}(\mathbf{k} + \mathbf{q}, i\omega_n) \left((\eta_{\mathbf{q}} - \bar{\eta}_{\mathbf{q}})^2 \mathcal{D}^{-(0)}(\mathbf{q}, 0) + (\eta_{\mathbf{q}} + \bar{\eta}_{\mathbf{q}})^2 \mathcal{D}^{+(0)}(-\mathbf{q}, 0) \right) \\ &= U^2 \frac{T}{N} \sum_{\mathbf{q}}' \frac{2(\bar{\eta}_{\mathbf{q}}^2 + \eta_{\mathbf{q}}^2)}{\Omega_{\mathbf{q}}} G^{v(0)}(\mathbf{k} + \mathbf{q}, i\omega_n) + \sum_{\mathbf{q}+\mathbf{Q}}' \frac{2(\bar{\eta}_{\mathbf{q}+\mathbf{Q}}^2 + \eta_{\mathbf{q}+\mathbf{Q}}^2)}{\Omega_{\mathbf{q}+\mathbf{Q}}} G^{v(0)}(\mathbf{k} + \mathbf{q} + \mathbf{Q}, i\omega_n) \\ &\approx U^2 T \frac{2}{JS} \frac{|\ln \epsilon|}{2\pi} G^{v(0)}(\mathbf{k}, i\omega_n) \end{aligned} \quad (10)$$

Here and below we define the sign of Σ by requesting that $G^{-1} = G_0^{-1} - \Sigma$.

In the second line of Eq. (10), we kept only the term with zero Matsubara frequency $\Omega_m = 0$, whereas in the last line we present the result of the momentum integration with logarithmical accuracy, using $\int d^2 \mathbf{q} \frac{1}{\Omega_{\mathbf{q}}} \sim$

$\int d^2 \mathbf{q} \frac{1}{|\mathbf{q}|} + \int d^2 \mathbf{q} \frac{1}{|\mathbf{q}-\mathbf{Q}|} \sim |\log \epsilon|$ (a more accurate result is $\log \pi / (\sqrt{2} |\epsilon|)$). The contribution to $\Sigma^{c(1)}$ from $G^{c(0)}$ is a subleading one, due to the gradient nature of the electron-magnon coupling for small momentum transfer.

Substituting the form of $G^{v(0)}(\mathbf{k}, i\omega_n)$ into (10), we find

$$\Sigma^{c(1)}(\mathbf{k}, i\omega_n) \approx \frac{\mathbb{T}^*(U/2)^2}{i\omega_n - (\epsilon_{\mathbf{k}}^v - \mu)}. \quad (11)$$

A similar analysis for valence fermions yields

$$\Sigma^{v(1)}(\mathbf{k}, i\omega_n) \approx \frac{\mathbb{T}^*(U/2)^2}{i\omega_n - (\epsilon_{\mathbf{k}}^c - \mu)}. \quad (12)$$

Treating Σ perturbatively as a correction to the Green's function near its mass shell, we find that at large U each self-energy changes the fermionic energy from $\epsilon^{c,v} \approx \pm U/2 + \mathcal{O}(t)$ to

$$\epsilon^{c,v} \approx \pm U \left(\langle S_z \rangle + \frac{\mathbb{T}^*}{4} \right) + \mathcal{O}(t) \quad (13)$$

Substituting $\langle S_z \rangle$ from (8), we find that the corrections of order \mathbb{T}^* cancel out, hence the energies of the conduction and valence fermions remain $\epsilon^{c,v} \approx \pm U/2$. This feature has been interpreted as an indication that the gap between the conduction and the valence bands is the Hubbard U , set by Mott physics, and it survives even when $\langle S_z \rangle$ vanishes, despite the fact that at the mean-field level this gap is defined as $2U\langle S_z \rangle$ [20, 45].

2. Paramagnetic state

Next, we consider the paramagnetic state at a finite temperature. To lowest order in U , the (Hartree-Fock)

self-energy is purely static and renormalizes the hoppings and the chemical potential. We move one step ahead and include into the self-energy multiple insertions of particle-hole bubbles. This effectively splits the interaction into charge and spin components. At the RPA level, the self-energy can be expressed as (Fig. 4(b))

$$\Sigma(\mathbf{k}, \omega_m) = -\frac{T}{2} \sum_{m,\beta} \int \frac{d^2\mathbf{q}}{(2\pi)^2} G(\mathbf{k} + \mathbf{q}, \omega_m + \Omega_m) \times \Gamma_{\alpha\beta;\beta\alpha}(\mathbf{q}, \Omega_m) \quad (14)$$

where

$$\Gamma_{\alpha\beta;\gamma\delta}(\mathbf{q}, \Omega_m) = \frac{U}{2} \left(\frac{\delta_{\alpha\beta}\delta_{\gamma\delta}}{1 + U\Pi^{(c)}(\mathbf{q}, \Omega_m)} - \frac{\vec{\sigma}_{\alpha\beta} \cdot \vec{\sigma}_{\gamma\delta}}{1 - U\Pi^{(s)}(\mathbf{q}, \Omega_m)} \right) \quad (15)$$

and $\Pi^{(c,s)}(q, \Omega_m)$ is the particle-hole bubble in the charge and spin channels [49]. For example, without coupling with collective excitations, $\Pi^{(c,s)}(q, \Omega_m)$ can be determined from the convolution of two free fermion propagators, and satisfies $\Pi^{(c)}(q, \Omega_m) = \Pi^{(s)}(q, \Omega_m) = \Pi(q, \Omega_m)$. Near a SDW instability at $U\Pi^{(s)}(Q, 0) = 1$, the dominant interaction comes from spin fluctuations. Dropping the charge component of Γ , we obtain an effective model with the interaction mediated by spin fluctuations. Approximating the static $1 - U\Pi^{(s)}(q)$ by Ornstein-Zernike form $1 - U\Pi^{(s)}(q) = \mathfrak{c}((\mathbf{q} - \mathbf{Q})^2 + \xi^{-2})$, where \mathfrak{c} is a dimensionless constant, we obtain the thermal self-energy at a hot spot in the form

$$\Sigma_{\text{para}}^{(1)}(\mathbf{k}_{hs}, i\omega_n) = 3\bar{g}T \int \frac{d\mathbf{q}}{(2\pi)^2} \frac{1}{i\omega_n - v_F\tilde{q}_\perp} \frac{1}{\tilde{q}_\perp^2 + \tilde{q}_\parallel^2 + \xi^{-2}} = -i \operatorname{sgn} \omega_m \frac{3\bar{g}T}{2\pi v_F \xi^{-1}} f\left(\frac{|\omega_n|}{v_F \xi^{-1}}\right). \quad (16)$$

where $\bar{g} \sim \mathfrak{c}^{-1}U$ is an effective coupling,

$$f(y) = \frac{1}{\sqrt{y^2 - 1}} \log\left(y + \sqrt{y^2 - 1}\right), \quad (17)$$

and the factor of 3 comes from spin summation. It is convenient to introduce the dimensionless coupling

$$\lambda = \frac{3\bar{g}T}{2\pi(v_F\xi^{-1})^2}. \quad (18)$$

and dimensionless frequency $\mathbf{w}_m = \omega_m/(v_F\xi^{-1})$. The Green's function is

$$G(\mathbf{k}_{hs}, \omega_m) = \left(iv_F \xi^{-1} \left(\mathbf{w}_m + \lambda \operatorname{sgn} \mathbf{w}_m \frac{\log\left(|\mathbf{w}_m| + \sqrt{(\mathbf{w}_m)^2 - 1}\right)}{\sqrt{(\mathbf{w}_m)^2 - 1}} \right) \right)^{-1}. \quad (19)$$

To see the effect of the self-energy, it is instructive to convert this expression onto the real axis, $i\omega_m \rightarrow \omega + i\delta$.

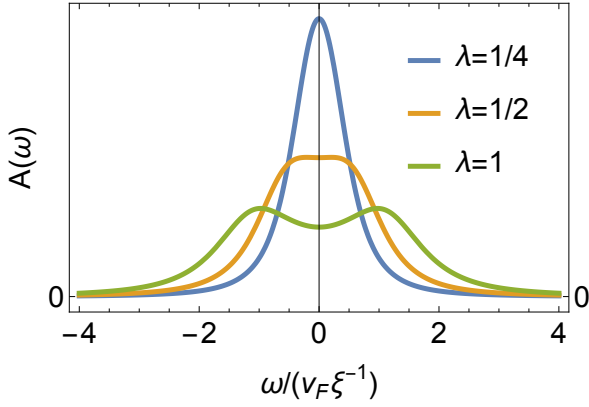


FIG. 5. Spectral function at the hot spot from the one-loop calculation (Eq. 21). As the dimensionless coupling $\lambda = \frac{3\bar{q}T}{2\pi(v_F\xi^{-1})^2}$ increases, the spectral function shows pseudogap behavior when $\lambda > \lambda_c = 0.47$.

The retarded self-energy is

$$\Sigma_{\text{para}}^{(1)}(\mathbf{k}_{hs}, \omega) = v_F \xi^{-1} \lambda \left(\frac{\log(w + \sqrt{w^2 + 1})}{\sqrt{w^2 + 1}} - i \frac{\pi/2}{\sqrt{w^2 + 1}} \right), \quad (20)$$

note that the real part of $\Sigma_{\text{para}}^{(1)}(\mathbf{k}_{hs}, \omega)$ is an odd function of w . The retarded Green's function is

$$G_{\text{ret}}(\mathbf{k}_{hs}, w) = \left(v_F \xi^{-1} \left(w - \lambda \frac{\log(w + \sqrt{w^2 + 1})}{\sqrt{w^2 + 1}} + i \lambda \frac{\pi/2}{\sqrt{w^2 + 1}} \right) \right)^{-1}. \quad (21)$$

We plot the spectral function $A(\mathbf{k}_{hs}, w) = -(1/\pi) \text{Im}G_{\text{ret}}(\mathbf{k}_{hs}, w)$ in Fig. 5. We see that at small λ , $A(\mathbf{k}_{hs}, w)$ is peaked at $w = 0$, as is expected for weakly interacting fermions with momenta at the Fermi surface. The key effect of the self-energy at these λ is to introduce a finite width of $A(\mathbf{k}_{hs}, w)$. However once λ exceeds the critical value $\lambda_c \approx 0.47$, the maximum of $A(\mathbf{k}_{hs}, w)$ shifts to a finite $|w| \sim \sqrt{\lambda - \lambda_c}$, while at zero frequency, $A(\mathbf{k}_{hs}, 0)$ now becomes a minimum (see Fig. 5). This implies that thermal fluctuations in the paramagnetic state do give rise to pseudogap behavior already at one-loop order, if the coupling exceeds the threshold value. We define the one-loop pseudogap as $\Delta_{\text{pg}}^{(1)}$.

At small frequencies, the evolution of the spectral function with increasing λ can be obtained analytically. Expanding $A(\mathbf{k}_{hs}, w)$ near $w = 0$, we obtain

$$A(\mathbf{k}_{hs}, w) = \frac{\lambda}{2v_F \xi^{-1}} \frac{1}{\frac{\pi^2 \lambda^2}{4} + w^2 \left((1 - \lambda)^2 - \frac{\lambda^2 \pi^2}{8} \right)} \quad (22)$$

We see that the maximum of $A(\mathbf{k}_{hs}, w)$ remains at $w = 0$ as long as $\lambda(1 + \pi/(2\sqrt{2})) < 1$. The critical value $\lambda_c = 2\sqrt{2}/(2\sqrt{2} + \pi) = 0.4738$.

We next consider large λ . We assume and then verify that the position of the maximum of $A(\mathbf{k}_{hs}, w)$ moves to $w \gg 1$, i.e., to $\omega \gg v_F \xi^{-1}$. For such w , the momentum integration in the expression for the self-energy is fully confined to the bosonic term $\frac{1}{\bar{q}_\perp^2 + \bar{q}_\parallel^2 + \xi^{-2}}$, while the fermionic Green's function can be moved out of the momentum integral. For the retarded self-energy we obtain for such w with logarithmic accuracy:

$$\Sigma_{\text{para}}^{(1)}(\mathbf{k}_{hs}, \omega) = v_F \xi^{-1} \lambda \left(\frac{\log w}{w} - i \frac{\pi}{2w} \right) \quad (23)$$

The retarded Green's function is

$$G_{\text{ret}}(\mathbf{k}_{hs}, w) = \left(v_F \xi^{-1} \left(w - \lambda \frac{\log(w)}{w} + i \lambda \frac{\pi}{2w} \right) \right)^{-1}, \quad (24)$$

and the spectral function is

$$A(\mathbf{k}_{hs}, w) = \frac{\lambda w}{2v_F \xi^{-1}} \frac{1}{\frac{\pi^2 \lambda^2}{4} + (w^2 - \lambda \log w)^2}. \quad (25)$$

This function has a maximum at $w \approx \left(\frac{\lambda \log \lambda}{2} \right)^{1/2}$. The corrections to this expression are of order $\log(\log(\lambda))$. They change the prefactor for λ under the logarithm to $\log(\mathfrak{b}(\lambda)\lambda)$, where $\mathfrak{b}(\lambda)$ is a slowly varying function of λ . In Fig. 6 we plot $\Delta_{\text{pg}}^{(1)}/(v_F \xi^{-1})$, which we obtained numerically, without expanding at large w , along with the analytical $\Delta_{\text{pg}}^{(1)}/(v_F \xi^{-1}) = (\lambda \log(\mathfrak{b}(\lambda)))^{1/2}$. We found a good match by setting $\mathfrak{b} = 14.8$ independent on λ . We emphasize that $\Delta_{\text{pg}}^{(1)}/(v_F \xi^{-1})$ is large at large λ , which justifies the assumption that we used to obtain (9).

Because $\lambda \propto \xi^{-2}$, the $(\lambda \log \lambda)^{1/2}$ dependence at large λ can be approximated by a more simple $\lambda |\log \xi|$, which is more convenient for calculations beyond one-loop order. In dimension $d = 2 + \epsilon$, $\log \xi$ is replaced by $L = 0.5 \log \frac{\pi^2}{2(\epsilon^2 + \xi^{-2})}$. Using these modifications and extending the result to \mathbf{k} near, but not necessary at a hot spot, we obtain at large λ

$$\Sigma_{\text{para}}^{(1)}(\mathbf{k}, \omega) \approx (v_F \xi^{-1})^2 \frac{\lambda L}{\omega - (\epsilon_{\mathbf{k}+\mathbf{Q}} - \mu)}. \quad (26)$$

At $\xi^{-1} = 0$, this expression has the same form as one-loop self-energy at the end point of the SDW state, Eqs. (11) and (12), once we set $\Delta \rightarrow 0^+$ and identify $\epsilon_{\mathbf{k}}^v \rightarrow \min\{\epsilon_{\mathbf{k}}, \epsilon_{\mathbf{k}+\mathbf{Q}}\}$, $\epsilon_{\mathbf{k}}^c \rightarrow \max\{\epsilon_{\mathbf{k}}, \epsilon_{\mathbf{k}+\mathbf{Q}}\}$. The prefactors in (26) and (11)-(12) match if we set the prefactor \mathfrak{c} in $(1 - U\Pi^{(s)}(\mathbf{q}, 0)) = \mathfrak{c}(\xi^{-2} + (\mathbf{q} - \mathbf{Q})^2)$ to be

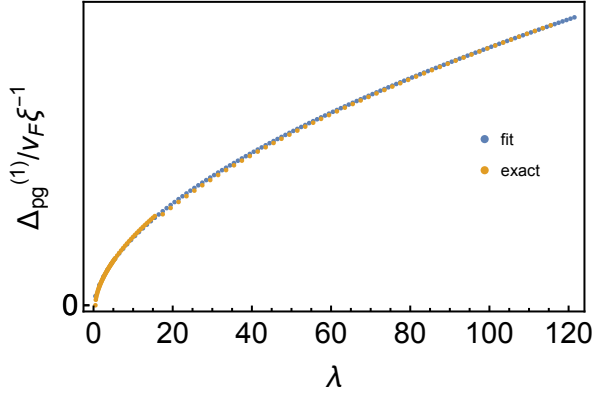


FIG. 6. The ratio of the pseudogap scale $\Delta_{\text{pg}}^{(1)}$, extracted from the one-loop Green's function, and $v_F \xi^{-1}$. Orange dots: the ratio, extracted from the numerical analysis of Eq. (21). Blue dots: the fit to the analytical expression $\Delta_{\text{pg}}^{(1)}/(v_F \xi^{-1}) = (\frac{1}{2} \lambda \log \mathfrak{b} \lambda)^{1/2}$. The best fit is for $\mathfrak{b} = 14.8$.

$\mathfrak{c} \sim J/U \sim (t/U)^2$. While $\mathfrak{c} \sim (t/U)^2$ holds deep in the SDW state when $\Delta \sim U/2$, we will not discuss here how to justify the expression for \mathfrak{c} in the paramagnetic state and use it as a phenomenological element of our analysis. With the choice of $\mathfrak{c} \sim J/U$ as the proper prefactor, the one-loop self-energy in the paramagnetic state at $|\omega - (\epsilon_{\mathbf{k}+\mathbf{Q}} - \mu)| \gg v_F \xi^{-1}$ is

$$\Sigma'_{\text{para}}(1)(\mathbf{k}, \omega) = \frac{\mathfrak{t}(U/2)^2}{\omega - (\epsilon_{\mathbf{k}+\mathbf{Q}} - \mu)}, \quad (27)$$

where

$$\mathfrak{t} = \frac{4T}{\pi JS} L = \frac{2T}{\pi JS} \ln \frac{\pi^2}{2(\epsilon^2 + \xi^{-2})}. \quad (28)$$

At $\xi^{-1} = 0$, this coincides with \mathfrak{t}^* from Eq. (9). The pseudogap energy $\Delta_{\text{pg}}^{(1)} = (U/2)\sqrt{\mathfrak{t}}$.

The correlation length at the one-loop order is given by

$$\xi = \left(\frac{A}{1 - U\Pi^{(s)}(\mathbf{Q}, 0)} \right)^{1/2}, \quad (29)$$

where the polarization bubble $\Pi^{(s)}(\mathbf{Q}, 0)$ is constructed out of Green's functions of free fermions. Evaluating $\Pi^{(s)}(\mathbf{Q}, 0)$ for $t - t'$ dispersion, we find that ξ is weakly temperature dependent. We label this correlation length as ξ_0 later in the text to distinguish it from the fully dressed ξ , which, as we will show, is strongly T -dependent.

B. Rational to go beyond one-loop analysis

We now rationalize the need to go beyond the one-loop analysis

For the SDW state, the one-loop formulas for $\langle S_z \rangle$ and for the self-energy are the leading terms in an expansion in \mathfrak{t}^* . Meanwhile, the SDW order vanishes at $T = T_N$, at which $\mathfrak{t}^* = O(1)$, as is clear from (8). To understand how $\langle S_z \rangle$ evolves at these \mathfrak{t}^* values, we clearly need to include terms beyond the one-loop order. The same holds for the fermionic self-energy, which also evolves at $\mathfrak{t}^* = O(1)$. One can easily verify that for both $\langle S_z \rangle$ and the self-energy, n -loop order terms are of order $(\mathfrak{t}^*)^n$, i.e., terms up to an infinite loop order have to be included in the analysis at $\mathfrak{t}^* = O(1)$.

The rational for the paramagnetic phase is similar. First, at $\mathfrak{t} = O(1)$, higher-loop diagrams for the thermal self-energy are of the same order as the one-loop one, and have to be kept. Second, the corrections to the polarization $\Pi^{(s)}(\mathbf{Q}, 0)$, which determines the correlation length via (29), also scale as powers of \mathfrak{t} and should all be kept at $\mathfrak{t} = O(1)$. In this respect, there is a similarity between the correlation length ξ in the paramagnetic state and $\langle S_z \rangle$ in the SDW state – both have to be computed by summing up infinite series in either \mathfrak{t} or \mathfrak{t}^* .

C. Infinite summation in the quasistatic limit

In this subsection, we collect contributions to order $(\mathfrak{t}^*)^m$ and \mathfrak{t}^m with m up to infinity and apply the eikonal formalism to obtain fully dressed variables.

For the SDW state, the diagrammatic series are determined kinematically by the structure of the electron-magnon coupling in Eqs. (6) and (7). We show below that the analysis of the full spectral function shows that there are two energy scales. One is the fully renormalized SDW order parameter $\Delta = U\langle S_z \rangle$, below which $A(k, \omega)$ vanishes, and the other is the pseudogap scale $\Delta_{\text{pg}}^{(e)}$, where the spectral function has a hump.

In the paramagnetic state, there are again two energy scales, the pseudogap $\Delta_{\text{pg}}^{(e)}$ in the full Green's functions, obtained in the eikonal approach, and $v_F \xi^{-1}$, where ξ is given by (29) with the fully renormalized polarization bubble. We show that $\Delta_{\text{pg}}^{(e)}$ is comparable to the one-loop $\Delta_{\text{pg}}^{(1)}$, but the full $\xi = \xi(T)$ differs from one-loop result and is strongly T -dependent.

1. SDW state

In the SDW state, the full Green's function $G^{c,v}$ with self-energy corrections to all loop orders reads

$$G^{c,v}(\mathbf{k}, i\omega_n) = G^{c,v(0)}(\mathbf{k}, i\omega_n) \sum_m \mathcal{C}_m \left(\mathbb{t}^* \frac{U^2}{4} \right)^m \times \left(G^{v,c(0)}(\mathbf{k}, i\omega_n) G^{c,v(0)}(\mathbf{k}, i\omega_n) \right)^m. \quad (30)$$

The combinatoric factor $\mathcal{C}_m = m!$ is determined by counting the number of non-equivalent diagrams of order $(\mathbb{t}^*)^m$ at the m -th loop order. The number is set by the structure of the fermion-magnon vertices in Eq. (7), which requires that each magnon propagator must be attached to one solid circle vertex (\bullet) and one empty circle vertex (\circ). This requirement is due to the spin conservation, i.e. the $U(1)$ spin rotation symmetry in the collinear SDW state. In Fig. 7, we show the diagrammatic series for the full Green's function up to three-loop order.

The series in Eq. (30) can be summed exactly by using $\mathcal{C}_m = \Gamma(m+1) = \int_0^\infty dx x^m e^{-x}$ and expressing the full Green's function in the integral form as

$$G^{c,v}(\mathbf{k}, \omega) = G^{c,v(0)}(\mathbf{k}, \omega) \int_0^\infty dt e^{-t} \frac{1}{1 - u_{\mathbf{k},\omega} t}, \quad (31)$$

where $u_{\mathbf{k},\omega} = \mathbb{t}^*(U/2)^2 G^{c(0)}(\mathbf{k}, \omega) G^{v(0)}(\mathbf{k}, \omega)$ and $G^{c,v(0)}$ are the bare Green's functions for conduction and valence fermions, but with the exact chemical potential

$\mu = \mu(x, T)$ and fully renormalized SDW order parameter $\Delta = \Delta(x, T) = U \langle S_z \rangle$. To determine the chemical potential and the SDW order parameter, we express the fermion density and $\Delta(x, T)$ in terms of the fermionic spectral functions $A_{\mathbf{k}}^{c,v}(\omega) = -\frac{1}{\pi} \text{Im} G^{c,v}(\mathbf{k}, \omega + i\delta)$ as [20]

$$\begin{aligned} \frac{1-x}{2} &= \int d\omega \int \frac{d^2\mathbf{k}}{(2\pi)^2} n_F(\omega) A_{\mathbf{k}}(\omega) \\ &= \int d\omega \int \frac{d^2\mathbf{k}}{(2\pi)^2} n_F(\omega) (u_{\mathbf{k}}^2 A^c(\mathbf{k}, \omega) + v_{\mathbf{k}}^2 A^v(\mathbf{k}, \omega)), \\ \langle S_z \rangle &= \int d\omega \int \frac{d^2\mathbf{k}}{(2\pi)^2} n_F(\omega) u_{\mathbf{k}} v_{\mathbf{k}} (A_{\mathbf{k}}^c(\omega) - A_{\mathbf{k}}^v(\omega)), \end{aligned} \quad (32)$$

where $n_F(\omega) = 1/(\exp(\omega/T) + 1)$ is the Fermi function, and the coherence factors $u_{\mathbf{k}}, v_{\mathbf{k}}$ are the same as in Eq. (4), but with Δ_0 in $E_{\mathbf{k}}$ replaced by $\Delta = \langle S_z \rangle / U$.

Solving Eq. (31) we find

$$G^{c,v}(\mathbf{k}, \omega) = G^{c,v(0)}(\mathbf{k}, \omega) \frac{e^{-1/u_{\mathbf{k},\omega}}}{u_{\mathbf{k},\omega}} \left(\text{Ci} \left(\frac{1}{u_{\mathbf{k},\omega}} \right) + \text{Si} \left(\frac{1}{u_{\mathbf{k},\omega}} \right) - i\pi \text{sgn} \left(\text{Im} \left(\frac{1}{u_{\mathbf{k},\omega}} \right) \right) \right), \quad (33)$$

where $\text{Ci}(\dots)$ and $\text{Si}(\dots)$ are CoshIntegral and SinhIntegral. Substituting the expression for $u_{\mathbf{k},\omega}$ and evaluating the imaginary part of the full Green's function, we obtain

$$A(\mathbf{k}, \omega) = \frac{|\bar{\omega} + \varepsilon_{\mathbf{k}}^-|}{\mathbb{t}^*(U/2)^2} \exp \left[-\frac{\bar{\omega}^2 - E_{\mathbf{k}}^2}{\mathbb{t}^*(U/2)^2} \right] \Theta(\bar{\omega}^2 - E_{\mathbf{k}}^2) \quad (34)$$

where $\bar{\omega} = \omega + \mu - \varepsilon_{\mathbf{k}}^+$, $E_{\mathbf{k}} = \sqrt{(\varepsilon_{\mathbf{k}}^-)^2 + \Delta^2}$, and we remind the reader that $\varepsilon_{\mathbf{k}}^+ = \frac{\varepsilon_{\mathbf{k}} + \varepsilon_{\mathbf{k}+\mathbf{Q}}}{2}$ and $\varepsilon_{\mathbf{k}}^- = \frac{\varepsilon_{\mathbf{k}} - \varepsilon_{\mathbf{k}+\mathbf{Q}}}{2}$. At a hot spot, $\varepsilon_{\mathbf{k}}^- = 0$, hence $E_{\mathbf{k}} = \Delta$, and $\bar{\omega} = \omega + \delta\mu$, where $\delta\mu = \mu - \mu_0$, the latter being the chemical po-

tential of free fermions. The spectral function as a function of $\bar{\omega}$ vanishes at $|\bar{\omega}| < \Delta$, and has a maximum at $|\bar{\omega}| = \Delta_{\text{pg}}^{(e)}$, where $\Delta_{\text{pg}}^{(e)} = \frac{1}{\sqrt{2}}(U/2)(\mathbb{t}^*)^{1/2}$. For $\Delta > \Delta_{\text{pg}}^{(e)}$, the spectral function shows two peaks at $\pm\Delta \approx \pm\Delta_0$ (see Fig. 1 (b)), and when $\Delta < \Delta_{\text{pg}}^{(e)}$, the spectral function vanishes below the SDW scale Δ and displays the humps at $\pm\Delta_{\text{pg}}^{(e)}$, which is comparable to Δ_0 . (see Fig. 1 (c)). In one further includes the non-thermal contribution to the fully renormalized fermion Green's function, finite jumps in the spectral function at $\bar{\omega} = \pm\Delta$ likely become the peaks [20]. Substituting the spectral function into (32), we find the self-consistent equations for $\mu(x, T)$ and $\Delta(x, T)$ in an integral form as

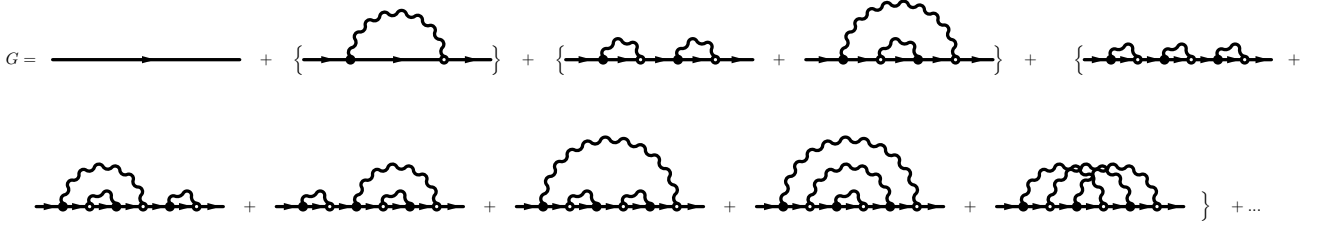


FIG. 7. Diagrammatic series for the full Green's function up to three loop order. In the SDW state, logarithmic corrections come from the transverse magnetic fluctuations, but not from the longitudinal ones. Keeping only transverse fluctuations, we obtain the combinatoric factor for the set of equivalent m -th order diagrams $C_m = m!$ (see the discussion below Eq. (30)). In the paramagnetic state, magnetic fluctuations are $SU(2)$ -symmetric, i.e., all three components of the magnetic susceptibility equally contribute to the self-energy. We verified, however, that the result for the self-energy does not change qualitatively if we only keep $n = 2$ components. In this case, for which we report the results, $C'_m = m!$ also in a paramagnetic state.

$$\frac{1-x}{2} = \int d\omega \int \frac{d\mathbf{k}}{(2\pi)^2} \frac{|\bar{\omega} + \varepsilon_{\mathbf{k}}^-|}{\mathbb{k}^*(U/2)^2} \exp\left[-\frac{\bar{\omega}^2 - E_{\mathbf{k}}^2}{\mathbb{k}^*(U/2)^2}\right] \Theta(\bar{\omega}^2 - E_{\mathbf{k}}^2) n_F(\omega) \quad (35)$$

$$\frac{1}{U} = \int d\omega \int \frac{d\mathbf{k}}{(2\pi)^2} \frac{-\text{sgn } \bar{\omega}}{\mathbb{k}^*(U/2)^2} \exp\left[-\frac{\bar{\omega}^2 - E_{\mathbf{k}}^2}{\mathbb{k}^*(U/2)^2}\right] \Theta(\bar{\omega}^2 - E_{\mathbf{k}}^2) n_F(\omega) \quad (36)$$

Analyzing the equations analytically, we find that the SDW gap at $T = 0$ splits at finite T into $\Delta_{\text{pg}}^{(e)}$, determined by the argument of the exponent in Eqs. (35) and (40), and Δ , determined by the Θ -function in Eq. (35).

We present the numerical results for $\Delta_{\text{pg}}^{(e)}$, Δ , and the spectral function in Sec. IV.

2. Paramagnetic state

In the paramagnetic state, the full Green's function is expressed as

$$G(\mathbf{k}, i\omega_n) = G^{(0)}(\mathbf{k}, i\omega_n) \sum_m C'_m \left(\frac{U^2}{4}\right)^m \times \left(G^{(0)}(\mathbf{k}, i\omega_n) G^{(0)}(\mathbf{k} + \mathbf{Q}, i\omega_n)\right)^m. \quad (37)$$

The combinatoric factor is determined by the number n of fluctuating spin components. For isotropic fluctuations, $n = 3$, and $C'_m = (2m + 1)!!$ [18, 20]; for transverse fluctuations, $n = 2$, and $C'_m = m!$, the same as in the SDW state. We verified that in both cases the system develops pseudogap behavior, the difference being only quantitative. Since the $n = 2$ case is simpler from computational perspective, below we present the results for $n = 2$ (the coupling λ for $n = 2$ is the same as in (18), but with the overall factor 2 instead of 3). The Green's function $G(\mathbf{k}, i\omega_n)$ can be presented in an integral form,

similar to Eq. (31):

$$G(\mathbf{k}, \omega) = G^{(0)}(\mathbf{k}, \omega) \int_0^\infty dt e^{-t} \frac{1}{1 - u_{\mathbf{k}, \omega} t}, \quad (38)$$

where $u_{\mathbf{k}, \omega} = \mathbb{k}(U/2)^2 G(\mathbf{k}, \omega) G(\mathbf{k} + \mathbf{Q}, \omega)$. Solving this equation, we obtain the spectral function

$$A(\mathbf{k}, \omega) = \frac{|\bar{\omega} + \varepsilon_{\mathbf{k}}^-|}{\mathbb{k}(U/2)^2} \exp\left[-\frac{\bar{\omega}^2 - (\varepsilon_{\mathbf{k}}^-)^2}{\mathbb{k}(U/2)^2}\right] \Theta(\bar{\omega}^2 - (\varepsilon_{\mathbf{k}}^-)^2), \quad (39)$$

where, we remind, $\bar{\omega} = \omega + \mu - \varepsilon_{\mathbf{k}}^+$. This spectral function has two unknowns: the chemical potential $\mu(x, T)$ and the spin correlation length $\xi(x, T)$, which appears in $\mathbb{k} \sim$

in ξ . One condition on μ and ξ is the constraint on the

fermion density

$$\frac{1-x}{2} = \int d\omega \int \frac{d\mathbf{k}}{(2\pi)^2} A(\mathbf{k}, \omega) n_F(\omega) = \int d\omega \int \frac{d\mathbf{k}}{(2\pi)^2} \frac{|\bar{\omega} + \varepsilon_{\mathbf{k}}^-|}{\mathbb{t}(U/2)^2} \exp\left[-\frac{\bar{\omega}^2 - (\varepsilon_{\mathbf{k}}^-)^2}{\mathbb{t}(U/2)^2}\right] \Theta(\bar{\omega}^2 - (\varepsilon_{\mathbf{k}}^-)^2) n_F(\omega). \quad (40)$$

To get the other condition, we relate ξ to the particle-hole polarization bubble in the same way as in the one-loop formula, $\xi = (A/(1 - U\Pi^{(s)}(\mathbf{Q}, 0)))^{1/2}$ (see Eq. (29) in Sec. III A 2), but including the series of thermal corrections into $\Pi^{(s)}(\mathbf{Q}, 0)$.

To evaluate $\Pi^{(s)}(\mathbf{Q}, 0)$, we note that both vertex corrections and corrections to the fermion Green's function should be included on an equal footing. The spin structure of the electron-magnon coupling implies that $\Pi^{(s)}(\mathbf{Q}, 0) = \Pi_{zz}(\mathbf{Q}, 0) = \Pi_{ss}(\mathbf{Q}, 0) - \Pi_{s\bar{s}}(\mathbf{Q}, 0)$, where $\Pi_{ss'}$ denotes the bubble diagram with spin indices s and s' at the two side vertices, and $s = \uparrow$, $\bar{s} = \downarrow$. We show the corresponding diagrams in Fig. 8. We find (see App. A for details)

$$\Pi^{(s)}(\mathbf{Q}, 0) = \frac{-1}{\mathbb{t}(U/2)^2} \int d\omega \int \frac{d\mathbf{k}}{(2\pi)^2} \left(n_F(\omega) \operatorname{sgn}(\bar{\omega}) \times \Theta(\bar{\omega} - (\varepsilon_{\mathbf{k}}^-)^2) \exp\left(-\frac{\bar{\omega}^2 - (\varepsilon_{\mathbf{k}}^-)^2}{\mathbb{t}(U/2)^2}\right) \right). \quad (41)$$

$$\begin{aligned} \Pi_{ss} &= \text{[diagram 1]} + 2 \text{[diagram 2]} + \\ &\quad \{ \text{[diagram 3]} + \text{[diagram 4]} + \text{[diagram 5]} \} + \dots \\ \Pi_{s\bar{s}} &= \text{[diagram 6]} + 4 \text{[diagram 7]} + \\ &\quad \{ \text{[diagram 8]} + \text{[diagram 9]} + 2 \text{[diagram 10]} + \dots \} + \dots \end{aligned}$$

FIG. 8. Diagrammatic series for the spin polarization bubble. The quantity we need is $\Pi^{(s)}(\mathbf{Q}, 0) = \Pi_{ss}(\mathbf{Q}, 0) - \Pi_{s\bar{s}}(\mathbf{Q}, 0)$, where $s = \uparrow$ and $\bar{s} = \downarrow$ are spin components at the two side vertices.

Note that because we included the same number $n = 2$ of fluctuating spin modes in the SDW and the paramagnetic state, the condition $\xi^{-1} = 0$, i.e., $\Pi^{(s)}(\mathbf{Q}, 0) = 1/U$, is equivalent to the condition on $\Delta = 0^+$ in Eq. (36).

We present the results in the next section. Before that, two comments are in order. First, the eikonal approach, which we employ here, is valid when the momentum integration in each diagram can be fully confined to the

bosonic propagator. This holds when the pseudogap energy $\Delta_{\text{pg}}^{(e)}$ (the half-distance between the humps in the full spectral function) found from the eikonal approach exceeds $v_F \xi^{-1}$. Once this condition breaks down, one can no longer pull out the Green's functions from the momentum integrals. In this situation, eikonal approach becomes uncontrollable. We will discuss this in more detail in the next section. Second, we re-iterate that for the fully self-consistent analysis, one should include longitudinal spin fluctuations across T_N . To account for these fluctuations in the SDW state, one would need to introduce another tunable parameter $\log \delta_{\text{amp}}$ for the amplitude mode.

We also note that Eqs. (34), (35) and (36) below T_N and Eqs. (39), (40) and (41) above T_N can be reproduced in the path-integral analysis, which maps the eikonal approximation onto the annealed disorder problem, similar to the discussions in Ref. [14, 18]. We discuss path-integral approach in Appendix A.

IV. RESULTS AND DISCUSSIONS

In this section, we present the solutions of Eqs. (34), (35) and (36) below T_N and Eqs. (39), (40) and (41) above T_N at the hole doping $x = 0.05$, for different values of the Hubbard U .

We present the results for (i) the spectral function $A(\omega)$, (ii) the spectral intensity $\bar{A}(\omega) = A(\omega)n_F(\omega)$, proportional to photoemission intensity, (iii) the SDW order parameter Δ , (iv) the pseudogap energy $\Delta_{\text{pg}}^{(e)}$, which is the half-distance between the two peaks in the spectral function, (v) the energy scale $v_F \xi^{-1}$ associated with magnetic fluctuations, (vi) the temperature dependence of the coupling constant $\lambda(T) \propto T/(v_F \xi^{-1})^2$, and (vii) the change of chemical potential, $\delta\mu = \mu - \mu_0$, we determine self-consistently from the condition that the total fermionic density equals $1 - x$.

In Fig. 9 we show the spectral function $A(\omega)$ (upper panel) and the spectral intensity $\bar{A}(\omega)$ (lower panel) for $U = 2\text{eV}$. The left and right panels show the results in the SDW state and the paramagnetic state, respectively. The spectral function in the SDW state has a true gap Δ and two maxima separated by $2\Delta_{\text{pg}}^{(e)} \sim U$.

The spectral intensity in both cases shows only a maximum (a pseudogap) at the energy $\omega = -(\Delta_{\text{pg}}^{(e)} + \delta\mu)$. At large U , $\Delta_{\text{pg}}^{(e)} \approx U/2$ and $\delta\mu \approx -U/2$, the sum is of order J . At intermediate $U = 2eV$, the frequency where $\bar{A}(\omega)$ has a maximum is comparable with Δ_0 . The shaded region in the paramagnetic state marks the condition $|\omega + \delta\mu| < v_F\xi^{-1}$, for which the eikonal approach is not applicable.

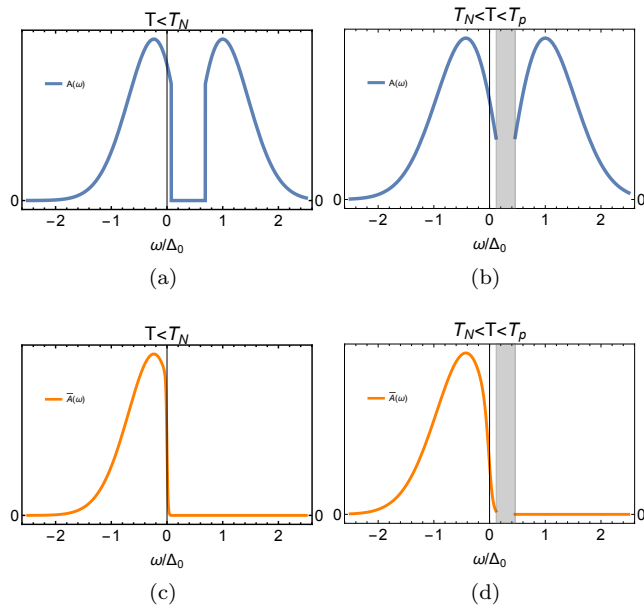


FIG. 9. Spectral function $A(\omega)$ (blue line in the upper panel) and spectral intensity $\bar{A}(\omega)$ (orange line in the lower panel) in (a,c) the SDW state for $T = 0.01\text{eV}$, from Eq. (34), and (b,d) the pseudogap regime for $T = 0.04\text{eV}$, from Eq. (39). We set $x = 0.05$, $U = 2\text{eV}$, $\epsilon = 0.01$ and $T_N = 0.013\text{eV}$. The gray shaded area in (b) is the region $|\omega + \delta\mu| < v_F\xi^{-1}$, where the eikonal approach breaks down.

In Fig. 10 we show how the different characteristic energies vary with temperature. The results for $U = 2\text{eV}$ and $U = 1\text{eV}$, for which the ground state is SDW ordered over a wide range of T , are shown in the left and middle columns. The bandwidth is set to be $W = 8t = 2.4\text{eV}$. In panels (a-b) we show the temperature evolution of Δ , $\Delta_{\text{pg}}^{(e)}$ and $v_F\xi^{-1}$ and in panels (d-e) we show the temperature dependence of the one-loop coupling constant $\lambda \propto T\xi^2$ (purple line) with $\xi(T)$, obtained by summing up eikonal series.

We see that the pseudogap does develop in the SDW state, and the pseudogap energy $\Delta_{\text{pg}}^{(e)}$ increases with T , roughly as \sqrt{T} , while the SDW order parameter Δ decreases with T and vanishes at T_N . Within our numerical accuracy the pseudogap becomes visible above a small, but finite T . Analytically, we found that it develops already at infinitesimally T .

In the paramagnetic phase above T_N , we find that

the pseudogap energy is quite flat (more so for larger $U = 2\text{eV}$). We call this a strong pseudogap behavior. Because the pseudogap energy $\Delta_{\text{pg}}^{(e)} \sim \sqrt{T \log \xi}$, the near temperature independence of $\Delta_{\text{pg}}^{(e)}$ implies that the fully renormalized ξ decreases rapidly, almost exponentially with $1/T$. In Fig. 11 we plot $\log \xi$ as a function of the inverse temperature. We see that the temperature evolution of $\log \xi$ is indeed nearly linear in $1/T$, i.e., to a reasonable accuracy, $\xi \sim e^{T_0/T}$. We emphasize that this result is obtained by computing ξ self-consistently from the four-point correlation function in the metallic state, which we compute by including self-energy and vertex corrections due to thermal magnetic fluctuations to all orders in perturbation theory. The exponential behavior mimics the one in the non-linear sigma model of localized spins [33, 50, 51], but we emphasize that we found this behavior in a metal. One specific indication of the distinction with localized spins is that in our case T_0 does not scale with $J \sim 1/U^2$ ($T_0 = 0.06\text{eV}$ for $U = 2\text{eV}$ and $T_0 = 0.04\text{eV}$ for $U = 1\text{eV}$).

For $U = 2\text{eV}$ the pseudogap energy $\Delta_{\text{pg}}^{(e)}$ remains larger than $v_F\xi^{-1}$ over the whole T range covered in Fig. 10, and in most of this range the system displays a strong pseudogap behavior.

For smaller $U = 1\text{eV}$, the condition $\Delta_{\text{pg}}^{(e)}$ remains larger than $v_F\xi^{-1}$ up to a certain $T_{\text{cross}} > T_N$ (Fig. 10 b). At larger T , eikonal approach breaks down. To understand the behavior at these T , we note that the actual pseudogap energy, Δ_{pg} , obtained from the full Green's function, is comparable to one-loop pseudogap energy $\Delta_{\text{pg}}^{(1)}$. The ratio of the latter and $v_F\xi^{-1}$ is controlled by the parameter λ , defined in (18) and is large when λ is large. Accordingly, the eikonal approach is valid when $\lambda \gg 1$. We plot $\lambda(T) \propto T\xi^2(T)$ in Fig. 10 (d, e), using $\xi(T)$ extracted from the fully dressed polarization bubble. We see that λ is indeed large when $\Delta_{\text{pg}} > v_F\xi^{-1}$. It diverges at the boundary of the SDW order where $\xi(T)$ diverges.

At $\lambda = O(1)$, we expect the one-loop expression for the self-energy to be sufficient, at least for qualitative reasoning. The one-loop pseudogap still exists at $\lambda \geq 1$, but the pseudogap energy $\Delta_{\text{pg}}^{(1)}$ decreases with decreasing λ and vanishes at $\lambda = \lambda_c = 0.47$ (see Fig. 2). We follow [17] and call this a weak pseudogap regime. In Fig. 12, we show the spectral function in both regimes. How far in T a weak pseudogap behavior extends depends on temperature variation of λ in the blue region in Fig. 10 (e), where the eikonal approach is no longer controllable, and the temperature variation of ξ cannot be obtained rigorously. Yet, we see from Fig. 10 (e) that λ still strongly decreases with T when $\Delta_{\text{pg}}^{(e)}$ and $v_F\xi^{-1}$ become comparable. It is then natural to assume that it continues decreasing at higher T and reaches critical λ_c

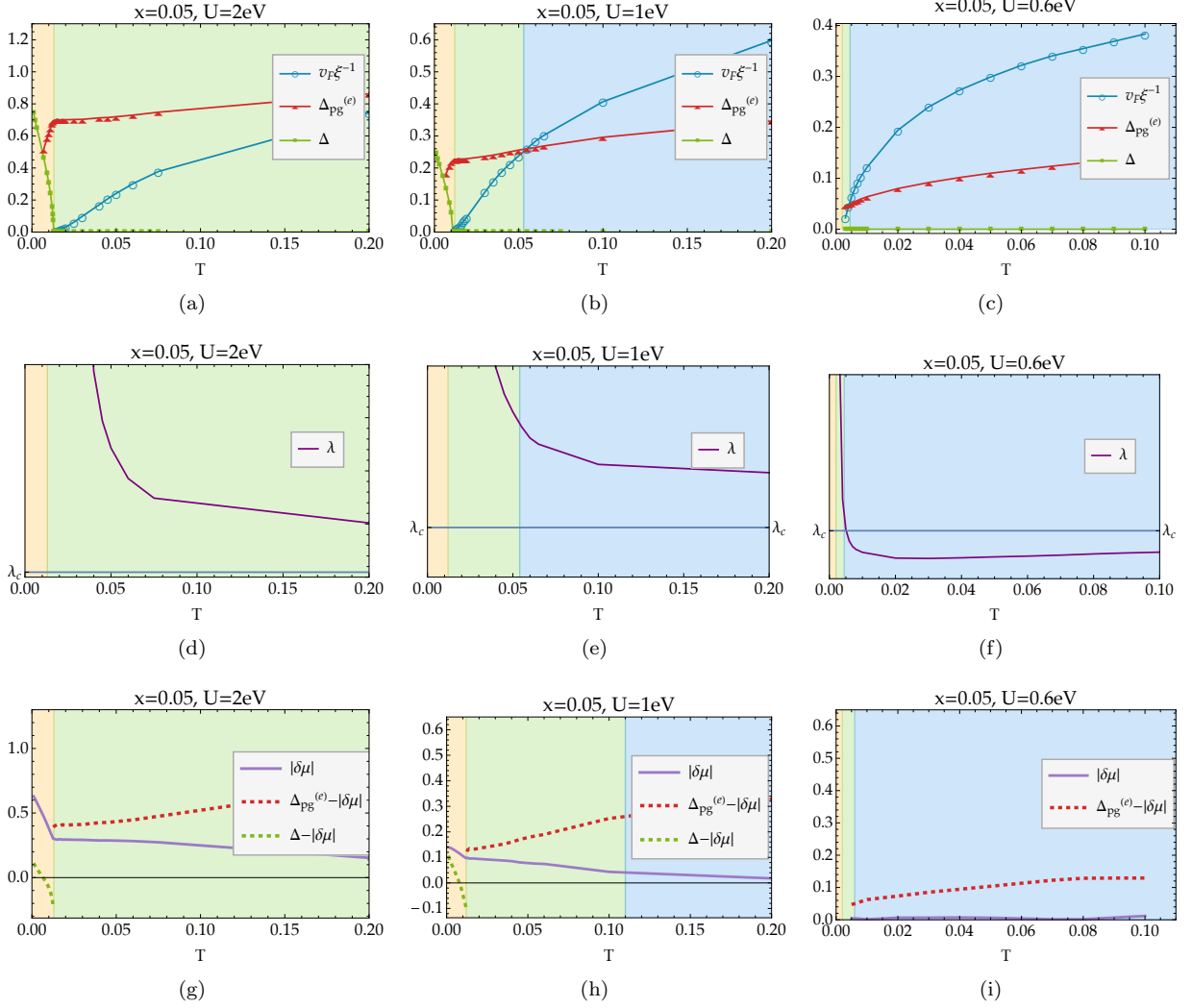


FIG. 10. Results for $U = 2.0\text{eV}$ (left column), $U = 1.0\text{eV}$ (middle column) and $U = 0.6\text{eV}$ (right column). We used $t = 0.3\text{eV}$, $t' = -0.06$, $x = 0.05$, $\epsilon = 0.01$. (a)-(c): Temperature evolution of the energy scales (in eV) Δ , $\Delta_{\text{pg}}^{(e)}$ and $v_F \xi^{-1}$. (d)-(f): Temperature evolution of $\lambda \propto T \xi^2$, which determines the behavior of the one-loop pseudogap $\Delta_{\text{pg}}^{(1)}$. Note that the numerical prefactors for λ are not taken into account in the plots. (g)-(i): Temperature evolution of the shifted chemical potential due to interaction, $\delta\mu = \mu - \mu_0$. The distances of the pseudogap and SDW gap from the chemical potential are plotted as $\Delta_{\text{pg}}^{(e)} - |\delta\mu|$ and $\Delta - |\delta\mu|$. Yellow, green, and blue areas denote, respectively, the SDW state, paramagnetic state with strong pseudogap behavior, and paramagnetic state with weak pseudogap behavior. The results in the blue shaded area are approximate as the eikonal approach breaks down in this region (see the text).

at some T_p . We expect a weak pseudogap behavior to exist also for $U = 2\text{eV}$, but at temperatures higher than the ones that we probe numerically.

Overall, for the values of U , for which the ground state is ordered, the pseudogap develops inside the SDW state, remains finite at T_N , persists into the paramagnetic phase and remains weakly T dependent up to $T_{\text{cross}} > T_N$. It then decreases with increasing T and eventually vanishes at $T = T_p$ (see Fig. 2). This behavior is quite consistent with the results of several numerical studies [32].

In panels (g-h) we show for these U the temperature evolution of the shift of the chemical potential $\delta\mu = \mu - \mu_0$, where, we remind, μ is the actual chemical potential and μ_0 is the chemical potential for free fermions. We emphasize that $\delta\mu$ is negative in the whole temperature range, where our approach is valid. In the same panels we plot $\Delta_{\text{pg}}^{(e)} - |\delta\mu|$ and $\Delta - |\delta\mu|$. When the difference is positive (which is the case for $\Delta_{\text{pg}}^{(e)} - |\delta\mu|$ for all T and for $\Delta - |\delta\mu|$ at low T), the spectral intensity $\bar{A}(\omega)$ at a hot spot has peaks at a negative ω , where $|\omega| = \Delta_{\text{pg}}^{(e)} - |\delta\mu|$ and $|\omega| = \Delta - |\delta\mu|$.

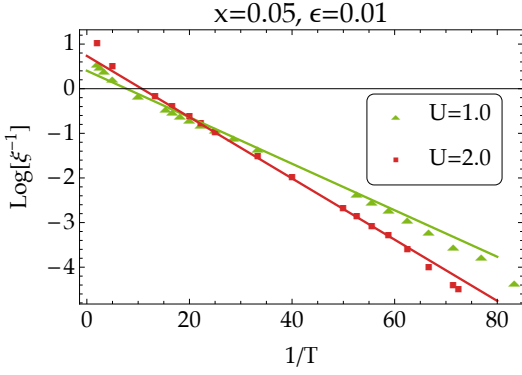


FIG. 11. Spin correlation length ξ as a function of temperature T . Over a temperature range (above T_N and when $\xi(T) \lesssim 1$), we find the fitting functions $\xi^{-1}(T) = 1.86e^{-\frac{0.06}{T-0.0015}}$ for $U = 2\text{eV}$ and $\xi^{-1}(T) = 1.26e^{-\frac{0.04}{T-0.0027}}$ for $U = 1\text{eV}$. The deviation from the 2D $n = 3$ non-linear sigma model (NLSM) behavior $\xi^{-1} \sim e^{-\rho_s/T}$ in the denominator of the exponential factor is due to the cutoff ϵ introduced in the computation, which is not relevant when $\epsilon < \xi^{-1}$ at $T > T_N$. At high temperature when $\xi \sim \mathcal{O}(1)$, the numerical results also deviate from the 2D NLSM behavior.

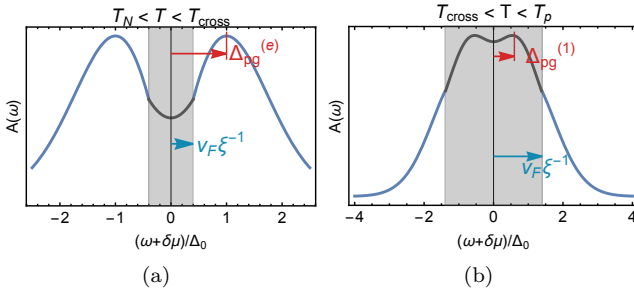


FIG. 12. The spectral function in the (a) strong pseudogap regime ($\Delta_{\text{pg}}^{(e)} > v_F \xi^{-1}$) and (b) weak pseudogap regime ($\Delta_{\text{pg}}^{(e)} < v_F \xi^{-1}$), where $\Delta_{\text{pg}}^{(e)}$ is the pseudogap obtained within the eikonal approach by summing up an infinite series of thermal contributions to the self-energy (blue solid line). The gray shaded area is the frequency range where the eikonal approach breaks down, and one should instead use the full one-loop result for the self-energy (gray solid line). $\Delta_{\text{pg}}^{(1)}$ is the pseudogap energy from such a one-loop calculation.

We next discuss what happens when the ground state is not ordered. We plot critical $U_c(x)$, at which the SDW order disappears at $T = 0$ at a given x , in Fig. 13. Note that this is the mean-field value of U_c as we consider only thermal fluctuations. For $x = 0.05$, $U_c = 0.58$. In panels (c,g,i) in Fig. 10 we present the results for $x = 0.05$ and $U = 0.6\text{eV}$, which is close to U_c . In numerical calculations we find no SDW order above $T \approx 0.002\text{eV}$ for this U , and very tiny SDW order $\Delta \approx 0.01\text{eV}$ at $T \leq 0.002\text{eV}$. Because both $\Delta_{\text{pg}}^{(e)}$, generated by thermal fluctuations, and ξ^{-1} necessary vanish at the SDW QCP, whether a strong pseudogap behavior exists at a finite T

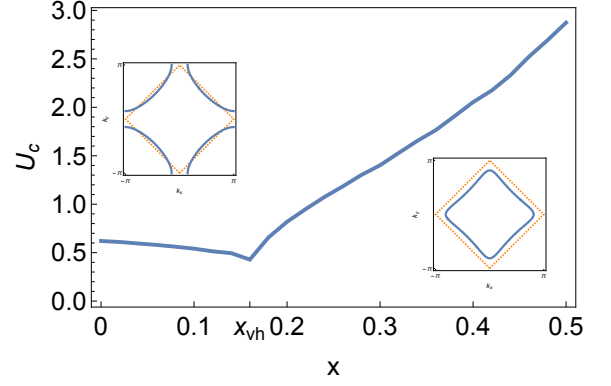


FIG. 13. Threshold U_c above which the (π, π) -SDW is a mean field solution at different doping x . U_c is the smallest at x_{vh} at which the Fermi surface changes topology. See figure insets for the Fermi surface (dark blue line) below x_{vh} (left inset) and above x_{vh} (right inset).

right above the QCP depends on the interplay between temperature variations of Δ_{pg} and $v_F \xi^{-1}$, and whether a weak pseudogap behavior exists depend on whether the temperature dependent coupling λ is larger than the critical λ_c . We see from Fig. 10 (c) that $v_F \xi^{-1} > \Delta_{\text{pg}}$ at all T , except the very lowest. We decreased U to U_c and to $0.57\text{eV} < U_c$ and verified that within our numerical accuracy, $\Delta_{\text{pg}} < v_F \xi^{-1}$ for all T . This implies that strong pseudogap behavior does not develop if there is no SDW order at $T = 0$. Furthermore, we see from Fig. 10 (f) that λ remains smaller than λ_c for all $T > 0.002\text{eV}$. We verified that at $U = U_c$, $\lambda < \lambda_c$ at all T within our numerical reach (see Fig. 14 b and discussions in Sec. IV A). Hence, a weak pseudogap behavior also does not develop if the ground state is not SDW-ordered. In other words, the pseudogap behavior holds only above the SDW ordering temperature $T_N(x)$, but does not extend to dopings, for which $T_N = 0$.

It is instructive to compare our results with the ones by Schmalian, Pines, and Stojković (SPS) (Ref. [18]), who also studied the evolution of the spectral function in the paramagnetic state in a non-perturbative fashion. SPS assumed that the static magnetic susceptibility can be factorized as

$$\chi(\vec{q} + \mathbf{Q}, 0) \sim \frac{1}{\xi^{-2} + \tilde{q}_{\parallel}^2 + \tilde{q}_{\perp}^2} \Rightarrow \frac{\xi^{-1}}{\xi^{-2} + \tilde{q}_{\parallel}^2} \frac{\xi^{-1}}{\xi^{-2} + \tilde{q}_{\perp}^2}. \quad (42)$$

This allowed them to obtain the iterative equation for the fermion Green's function between j th and $(j+1)$ th loop orders and sum up the contributions from all loop orders. In the limit $v_F \xi^{-1} \ll \Delta_{\text{pg}}$, their and our approaches yield the same diagrammatic series for G , whereas for $v_F \xi^{-1} \gg \Delta_{\text{pg}}$, the two results agree up to a numerical factor. The advantage of the SPS approach, based

on (42), is in that it allows one to analyze analytically the crossover between the strong and weak pseudogap regimes. The disadvantage is that it does not allow one to connect to pseudogap behavior in the SDW phase, because when $\xi \rightarrow \infty$ it yields $\int d^2\mathbf{q}\chi(\tilde{\mathbf{q}} + \mathbf{Q}, 0) = O(1)$ instead of divergent $\int d^2\mathbf{q}\chi(\tilde{\mathbf{q}} + \mathbf{Q}, 0) \sim \log \xi$, which we obtained without factorization. We also note that SPS took ξ as an input parameter, while we compute it self-consistently, in the same eikonal-type approach. This is essential for the understanding of the temperature evolution of Δ_{pg} in the paramagnetic phase. In particular, we argue in the next section that temperature dependence of the fully dressed ξ is such that pseudogap does not develop if the ground state is *not* magnetically ordered.

A. Phase diagram

To convert our results into the phase diagram in the (T, x) plane, we need to locate the parameter range where the thermal contribution to the self-energy is larger than the combined contribution from non-zero bosonic Matsubara frequencies. For systems with localized spins, there is no such regime as ξ^{-1} is linear in T , and for typical momenta $q \sim \xi^{-1}$, the static part of the inverse bosonic propagator $\xi^{-2} + q^2$ has the same T^2 temperature dependence as the dynamical $\omega_m^2 \sim T^2$ term. Then thermal and quantum fluctuations are comparable in strength in the whole low-energy range above a QCP. The phase diagram contains an ordered phase, a renormalized classical phase adjacent to it, a quantum-critical phase, where $\xi^{-1} \propto T$, and a quantum-disordered phase [33]. For metals with dynamical exponent $z = 1$ (the case when Landau damping of critical fluctuations is absent by kinematic reasons) the phase diagram is similar, with an extra region of Fermi-liquid phase on the paramagnetic side of the QCP.

For metals with $z > 1$, the static part of the inverse bosonic propagator scales as ξ^{-2} , for typical momenta $q \sim \xi^{-1}$, while the dynamical part scales as $T^{2/z}$. The two T dependencies are generally different, even if $\xi^{-1} \sim T$. At small T , it is natural to expect that ξ^{-2} is smaller than properly normalized $T^{2/z}$. Then thermal fluctuations give the largest contribution to the self-energy. As T increases, this condition $\xi^{-2} < T^{2/z}$ may or may not hold, depending on the thermal evolution of ξ . If it holds for all T , where the low-energy description is applicable, thermal fluctuations completely determine system behavior above a QCP. If it breaks down at some $T = T_q$ within the low-energy regime, then at this temperature the system crosses over from thermal fluctuations dominated non-Fermi liquid behavior at $T < T_q$ to still non-Fermi liquid behavior, but with the largest con-

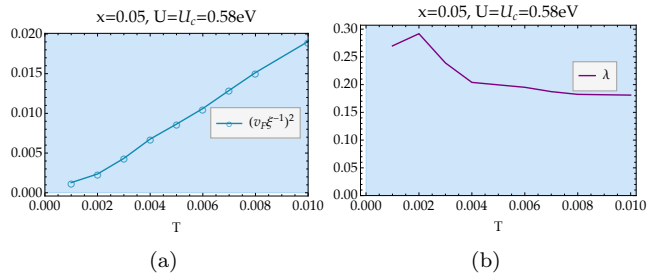


FIG. 14. (a) $(v_F \xi)^{-2}$ (b) $\lambda \propto T \xi^2$ as functions of temperature at the critical $U_c = 0.58\text{eV}$ for doping $x = 0.05$.

tribution to the self-energy coming from the terms with a non-zero bosonic Matsubara frequency.

This reasoning holds when in the thermal regime the system displays a pseudogap behavior (strong or weak). Otherwise, thermal fluctuations do not take the system out of a conventional Fermi liquid regime. In our notations, this implies that T_q must be smaller, or, at most, compatible to T_p .

To compare the two temperatures, we note that T_p corresponds to $\lambda = \lambda_c$. Using the definition of $\lambda = \lambda(T)$, Eq. (18), we find that T_p is the solution of $T_p \xi^2(T_p) \sim v_F^2/\bar{g}$. The temperature T_q is determined by comparing the Landau damping term at $\omega \sim T$ and $q \sim \xi^{-1}$ to ξ^{-2} . The Landau damping of spin excitations comes from scattering into low-energy fermions, and the effective coupling for this process is the same \bar{g} as in Eq. (26) for the self-energy. Evaluating the Landau damping term, we find that the equation on T_q is, up to a numerical factor, the same as for T_p : $T_q \xi^2(T_q) \sim v_F^2/\bar{g}$. Then T_q and T_p are comparable, i.e., the thermal region is also the pseudogap region.

Whether T_p is finite right above the SDW QCP depends on the temperature variation of $\xi^{-2}(T)$. If this variation was analytic $\xi^{-2}(T) \sim T^2$, the coupling $\lambda \propto T \xi^2(T)$ would necessarily be large at small T , and hence T_p would be finite. In this situation the pseudogap region would extend into the doping range where the ground state is not magnetically ordered. We find however, that above the SDW QCP, $\xi^{-2} \propto T$ (see Fig. 14 a) In this case, λ becomes T independent, and pseudogap develops if this constant λ is larger than λ_c and does not develop if it is smaller. As we already said, our results show that $\lambda < \lambda_c$ (see Fig. 14 b), hence pseudogap does not develop right above the QCP. By continuity, it also does not exist in the range where the ground state is not magnetically ordered. We caution, however, that this result is likely model-dependent, and in principle, there may be a situation when the magnitude of λ above a QCP extends λ_c . In such a case the pseudogap extends into the range where the ground state is not ordered.

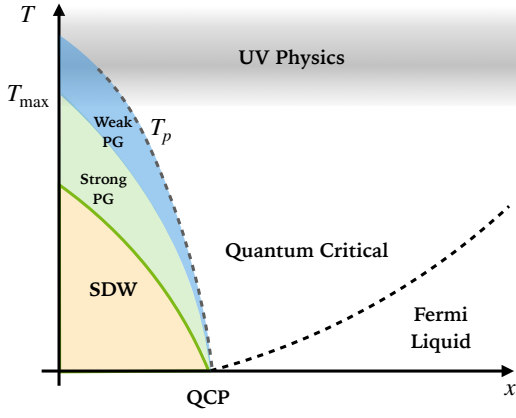
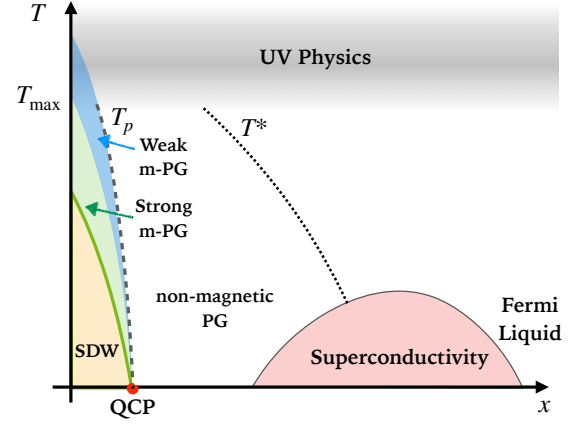


FIG. 15. A schematic phase diagram, obtained from our calculations (see Sec. IV A). A QCP corresponds to $x = x_c$ ($U = U_c(x)$). There is a SDW order at smaller x (larger U) and paramagnetic behavior holds for larger x (smaller U). Pseudogap develops in the regime, where the thermal contribution to the self-energy (the one from zero bosonic Matsubara frequency) is larger than the quantum one. The temperature T_p , where pseudogap disappears, roughly coincides with the boundary of the thermal region. In the quantum-critical region, thermal and quantum contributions to the self-energy are comparable in strength. In the Fermi liquid region, $\text{Im } \Sigma(\omega) \propto \omega^2$.

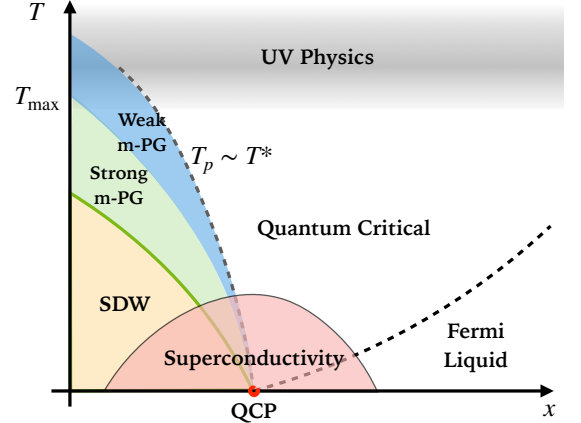
The linear in T behavior of ξ^{-2} above a QCP (modulo $\log T$) holds in the Hertz-Millis theory of the SDW quantum criticality [52], where it appears due to thermal bosonic self-energy from the phenomenologically introduced mode-mode coupling. In a microscopic theory, mode-mode coupling appears as an effective 4-boson interaction – a square made out of four fermionic propagators. The contribution from this effective interaction to bosonic self-energy is the same one as from inserting self-energy and vertex corrections into the polarization bubble [25], which are elements of our diagrammatic series for the fully dressed ξ . Not surprisingly then, we obtain the same linear in T dependence of ξ^{-2} as in Hertz-Millis theory. We note, however, that we collected infinite number of graphs for the bosonic propagator, not only the lowest order vertex and self-energy corrections.

We are now in position to obtain the phase diagram in variables x and T . For this, we combine our results (i) that there is no pseudogap at $T = 0$ from dynamical fluctuations, (ii) that the pseudogap behavior at a finite T exists only for $x < x_c$, when there is a SDW order in the ground state, (iii) that there is a quantum-critical behavior at $T > T_p$, and (iv) that at $x > x_c$ there is a Fermi liquid behavior at the smallest T . We show the phase diagram in Fig. 15.

In the two panels in Fig. 16 we present the phase diagrams for the cuprates, suggested by our study. In both figures pseudogap behavior due to thermal magnetic fluctuations exists only when the system has a SDW (π, π) order at $T = 0$.



(a)



(b)

FIG. 16. Two possible phase diagrams for the cuprates, based on our calculations. In both diagrams, the pseudogap behavior due to thermal magnetic fluctuations, denoted as “m-PG”, develops only above the (π, π) ordered state. In the strong pseudogap regime (Strong m-PG), the pseudogap energy weakly depends on temperature, while in the weak pseudogap regime (Weak m-PG), it decreases with increasing T and vanishes at T^* . In (a), SDW order holds only at x far smaller than the one for an optimal doping. This mimics the case of hole-doped cuprates. We conjecture that the pseudogap behavior, observed in hole-doped cuprates below $T^*(x)$, which extends to near-optimal doping, is either a precursor to superconductivity or a different state of matter, possibly with a topological order. In (b), SDW order extends to near-optimal doping, and the boundary of the magnetic pseudogap, T_p , becomes close T^* . In this situation, the experimentally detected pseudogap behavior well may be due to thermal spin fluctuations. This, we believe, mimics the case of electron-doped cuprates.

fluctuations exists only when the system has a SDW (π, π) order at $T = 0$. In Fig. 16 (a) this range is narrow and ends well before optimal doping. This phase diagram is likely applicable to hole-doped cuprates, where SDW region is quite narrow. We argue therefore that the pseudogap behavior, observed in these systems, is not caused

by thermal spin fluctuations and is instead either a precursor to superconductivity [12–16], or a novel state of matter with current-like or topological order [5–11]. In the phase diagram in Fig. 16b, the range of SDW order is wider and extends to near-optimal doping. In this case pseudogap behavior due to thermal magnetic fluctuations exists in a wider parameter range, and T_p , up to which it holds, may be close to the experimental boundary of the pseudogap phase. This last behavior holds in electron-doped cuprates [23], and we believe that pseudogap behavior, observed in these materials, may actually be due to thermal spin fluctuations.

A comment is in order here. In this paper we restricted our analysis to (π, π) SDW order. The recent numerical study [36] suggested that the pseudogap may exist as long as the ground state has a stripe magnetic order, which can be viewed as partly melted incommensurate $(\pi, Q)/(Q, \pi)$ SDW order [36, 40, 53–57]. Such an order has been extensively studied, chiefly in La-based cuprates (see e.g., [58, 59] and references therein). This may potentially widen the range of magnetically induced pseudogap behavior even in hole-doped cuprates.

V. SUMMARY

To summarize, in this paper, we analyzed the precursor scenario for pseudogap behavior of interacting fermions near a magnetic instability. We considered the Hubbard model on the square lattice and analyzed the thermal evolution of the spectral function. We adopted the eikonal-type approach, and summed up thermal contributions to the fermion two-point and four-point correlation functions to infinite order both in the SDW-ordered state and in the paramagnetic state. In the latter, the eikonal-type computational procedure is valid at large enough magnetic correlation lengths, which we compute self-consistently. For Hubbard U values comparable to the fermionic bandwidth, we found pseudogap behavior due to magnetic fluctuations and identified two different regimes: strong pseudogap behavior, which emerges after the summation of an infinite series of thermal contributions to two-point and four-point correlation functions, and weak pseudogap behavior, which emerges in the parameter range where the one-loop approximation is adequate. In the strong pseudogap regime we found that the magnetic correlation length decreases with T nearly exponentially, as $e^{T_0/T}$, such that the pseudogap energy scale $\Delta_{pg} \propto T \log \xi$ is almost independent on T , despite that it originates from thermal fluctuations. The near-exponential decrease of ξ mimics the behavior in the nonlinear sigma model of localized spins, but we emphasize that we obtained this behavior in a metal with strong

correlations. The near-independence of the pseudogap energy on T is consistent with numerical studies of the Hubbard model in the regime where the ground state is SDW-ordered (Ref. [32]). At higher T and higher dopings x , we found the crossover to the weak pseudogap regime, in which the pseudogap energy gradually decreases with increasing T or x and eventually vanishes at T_p .

Our calculations showed that the pseudogap behavior exists only above SDW ordering temperature and does not extend to dopings, where the ground state is disordered. This in turn is consistent with quantum Monte Carlo studies of the effective models of fermions interacting with magnetic fluctuations, as these studies didn't detect pseudogap behavior in the parameter range where the ground state is not magnetically ordered [34, 35, 38]. We presented in Fig. 15 the phase diagram based on our model calculations and presented in Fig. 16 the phase diagram for the cuprates. We argue that the magnetic pseudogap covers the range, where the pseudogap behavior has been detected in electron-doped cuprates, but does not cover the range of the observed pseudogap behavior in hole-doped cuprates. The pseudogap behavior in the latter is then either due to superconducting precursors, or is a novel ordered state. We note, however, that we didn't analyze a potential pseudogap behavior above a stripe order [36].

The last remark. In this paper we used the eikonal approach and set the limit of its applicability at $\Delta_{pg}^{(e)} \sim v_F \xi^{-1}$. The eikonal approach treats vertex and self-energy corrections equally, and the applicability limit is the same for both types of diagrams. It is possible that there exists an intermediate regime of $\Delta_{pg}^{(e)} \sim v_F \xi^{-1}$, where self-energy corrections are numerically stronger. In this situation, one has to include infinite series of self-energy corrections to the fermionic Green's function without including vertex corrections. This is equivalent to evaluating the Green's function in the self-consistent one-loop approximation (the self-energy is given by one-loop diagram, but with the full Green's function without vertex corrections of an internal fermion). Such an approximation has been widely used in the context of large-N limit of the SYK model and its variations [60]. The spectral function, obtained within the self-consistent one-loop approximation gets broadened compared to the spectral function of free fermions, but the peak of $A(k_F, \omega)$ remains at $\omega = 0$, the pseudogap *does not* develop. The analysis of the interplay between the eikonal and self-consistent one-loop approximation is somewhat involved and will be discussed separately.

ACKNOWLEDGMENTS

We thank Leon Balents, Erez Berg, Antoine Georges, Patrick Lee, Izabella Lovas, Subir Sachdev and Fedor Simkovic for helpful discussions. M.Y. was supported by the Gordon and Betty Moore Foundation through Grant GBMF8690 to UCSB, by a grant from the Simons

Foundation (216179, LB), and by the National Science Foundation under Grant No. NSF PHY-1748958. ZW and RMF were supported by the Department of Energy through the University of Minnesota Center for Quantum Materials, under Grant No. DE-SC-0016371. AVC was supported by the U.S. Department of Energy, Office of Science, Basic Energy Sciences, under Award No. DE-SC0014402.

-
- [1] M. A. Metlitski and S. Sachdev, Quantum phase transitions of metals in two spatial dimensions. ii. spin density wave order, *Phys. Rev. B* **82**, 075128 (2010).
- [2] Y. Wang and A. Chubukov, Charge-density-wave order with momentum $(2q, 0)$ and $(0, 2q)$ within the spin-fermion model: Continuous and discrete symmetry breaking, preemptive composite order, and relation to pseudogap in hole-doped cuprates, *Phys. Rev. B* **90**, 035149 (2014).
- [3] D. Chowdhury and S. Sachdev, Feedback of superconducting fluctuations on charge order in the underdoped cuprates, *Phys. Rev. B* **90**, 134516 (2014).
- [4] W. A. Atkinson, A. P. Kampf, and S. Bulut, Charge order in the pseudogap phase of cuprate superconductors, *New Journal of Physics* **17**, 013025 (2015).
- [5] C. M. Varma, Non-fermi-liquid states and pairing instability of a general model of copper oxide metals, *Phys. Rev. B* **55**, 14554 (1997).
- [6] C. M. Varma, Pseudogap phase and the quantum-critical point in copper-oxide metals, *Phys. Rev. Lett.* **83**, 3538 (1999).
- [7] S. Sachdev, Topological order, emergent gauge fields, and fermi surface reconstruction, *Reports on Progress in Physics* **82**, 014001 (2018).
- [8] Y.-H. Zhang and S. Sachdev, From the pseudogap metal to the fermi liquid using ancilla qubits, *Phys. Rev. Res.* **2**, 023172 (2020).
- [9] Y.-H. Zhang and S. Sachdev, Deconfined criticality and ghost fermi surfaces at the onset of antiferromagnetism in a metal, *Phys. Rev. B* **102**, 155124 (2020).
- [10] E. Mascot, A. Nikolaenko, M. Tikhonovskaya, Y.-H. Zhang, D. K. Morr, and S. Sachdev, Electronic spectra with paramagnon fractionalization in the single-band hubbard model, *Phys. Rev. B* **105**, 075146 (2022).
- [11] A. Nikolaenko, J. von Milczewski, D. G. Joshi, and S. Sachdev, Spin density wave, Fermi liquid, and fractionalized phases in a theory of antiferromagnetic metals using paramagnons and bosonic spinons, arXiv e-prints , arXiv:2211.10452 (2022), [arXiv:2211.10452 \[cond-mat.str-el\]](https://arxiv.org/abs/2211.10452).
- [12] M. R. Norman, M. Randeria, H. Ding, and J. C. Campuzano, Phenomenology of the low-energy spectral function in high- T_c superconductors, *Phys. Rev. B* **57**, R11093 (1998).
- [13] M. Franz and A. J. Millis, Phase fluctuations and spectral properties of underdoped cuprates, *Phys. Rev. B* **58**, 14572 (1998).
- [14] E. Berg and E. Altman, Evolution of the fermi surface of d -wave superconductors in the presence of thermal phase fluctuations, *Phys. Rev. Lett.* **99**, 247001 (2007).
- [15] Y.-M. Wu, S.-S. Zhang, A. Abanov, and A. V. Chubukov, Interplay between superconductivity and non-fermi liquid behavior at a quantum-critical point in a metal. v. the γ model and its phase diagram: The case $\gamma = 2$, *Phys. Rev. B* **103**, 184508 (2021).
- [16] X. Wang and Y. Qi, Phase Fluctuations in Two-Dimensional Superconductors and Pseudogap Phenomenon, arXiv e-prints , arXiv:2212.05737 (2022), [arXiv:2212.05737 \[cond-mat.supr-con\]](https://arxiv.org/abs/2212.05737).
- [17] J. Schmalian, D. Pines, and B. Stojković, Weak pseudogap behavior in the underdoped cuprate superconductors, *Phys. Rev. Lett.* **80**, 3839 (1998).
- [18] J. Schmalian, D. Pines, and B. Stojković, Microscopic theory of weak pseudogap behavior in the underdoped cuprate superconductors: General theory and quasiparticle properties, *Phys. Rev. B* **60**, 667 (1999).
- [19] É. Z. Kuchinskii and M. V. Sadovskii, Models of the pseudogap state of two-dimensional systems, *Journal of Experimental and Theoretical Physics* **88**, 968 (1999).
- [20] T. A. Sedrakyan and A. V. Chubukov, Pseudogap in underdoped cuprates and spin-density-wave fluctuations, *Phys. Rev. B* **81**, 174536 (2010).
- [21] M. Ye and A. V. Chubukov, Hubbard model on a triangular lattice: Pseudogap due to spin density wave fluctuations, *Phys. Rev. B* **100**, 035135 (2019).
- [22] A. Damascelli, Z. Hussain, and Z.-X. Shen, Angle-resolved photoemission studies of the cuprate superconductors, *Rev. Mod. Phys.* **75**, 473 (2003).
- [23] N. P. Armitage, P. Fournier, and R. L. Greene, Progress and perspectives on electron-doped cuprates, *Rev. Mod. Phys.* **82**, 2421 (2010).
- [24] D. J. Scalapino, A common thread: The pairing interaction for unconventional superconductors, *Rev. Mod. Phys.* **84**, 1383 (2012).
- [25] A. Abanov, A. V. Chubukov, and J. Schmalian, Quantum-critical theory of the spin-fermion model and its application to cuprates: Normal state analysis, *Advances in Physics* **52**, 119 (2003), <https://doi.org/10.1080/0001873021000057123>.

- [26] Y. M. Vilk and A. M. S. Tremblay, Destruction of fermi-liquid quasiparticles in two dimensions by critical fluctuations, *Europhysics Letters* **33**, 159 (1996).
- [27] A. V. Chubukov, M. R. Norman, A. J. Millis, and E. Abrahams, Gapless pairing and the fermi arc in the cuprates, *Phys. Rev. B* **76**, 180501 (2007).
- [28] A.-M. S. Tremblay, B. Kyung, and D. Sénéchal, Pseudogap and high-temperature superconductivity from weak to strong coupling. towards a quantitative theory (review article), *Low Temperature Physics* **32**, 424 (2006), <https://doi.org/10.1063/1.2199446>.
- [29] O. Gunnarsson, T. Schäfer, J. P. F. LeBlanc, E. Gull, J. Merino, G. Sangiovanni, G. Rohringer, and A. Toschi, Fluctuation diagnostics of the electron self-energy: Origin of the pseudogap physics, *Phys. Rev. Lett.* **114**, 236402 (2015).
- [30] J. P. F. LeBlanc, A. E. Antipov, F. Becca, I. W. Bulik, G. K.-L. Chan, C.-M. Chung, Y. Deng, M. Ferrero, T. M. Henderson, C. A. Jiménez-Hoyos, E. Kozik, X.-W. Liu, A. J. Millis, N. V. Prokof'ev, M. Qin, G. E. Scuseria, H. Shi, B. V. Svistunov, L. F. Tocchio, I. S. Tupitsyn, S. R. White, S. Zhang, B.-X. Zheng, Z. Zhu, and E. Gull (Simons Collaboration on the Many-Electron Problem), Solutions of the two-dimensional hubbard model: Benchmarks and results from a wide range of numerical algorithms, *Phys. Rev. X* **5**, 041041 (2015).
- [31] W. Wu, M. Ferrero, A. Georges, and E. Kozik, Controlling feynman diagrammatic expansions: Physical nature of the pseudogap in the two-dimensional hubbard model, *Phys. Rev. B* **96**, 041105 (2017).
- [32] T. Schäfer, N. Wentzell, F. Šimkovic, Y.-Y. He, C. Hille, M. Klett, C. J. Eckhardt, B. Arzhang, V. Harkov, F. m. c.-M. Le Régent, A. Kirsch, Y. Wang, A. J. Kim, E. Kozik, E. A. Stepanov, A. Kauch, S. Andergassen, P. Hansmann, D. Rohe, Y. M. Vilk, J. P. F. LeBlanc, S. Zhang, A.-M. S. Tremblay, M. Ferrero, O. Parcollet, and A. Georges, Tracking the footprints of spin fluctuations: A multimethod, multimessenger study of the two-dimensional hubbard model, *Phys. Rev. X* **11**, 011058 (2021).
- [33] S. Sachdev, *Quantum Phase Transitions* (Cambridge University Press, 2009).
- [34] M. H. Gerlach, Y. Schattner, E. Berg, and S. Trebst, Quantum critical properties of a metallic spin-density-wave transition, *Phys. Rev. B* **95**, 035124 (2017).
- [35] A. Klein, A. V. Chubukov, Y. Schattner, and E. Berg, Normal state properties of quantum critical metals at finite temperature, *Phys. Rev. X* **10**, 031053 (2020).
- [36] IV, Fedor Šimkovic and Rossi, Riccardo and Ferrero, Michel, Two-dimensional hubbard model at finite temperature: Weak, strong, and long correlation regimes, *Phys. Rev. Res.* **4**, 043201 (2022).
- [37] M. R. Norman, D. Pines, and C. Kallin, The pseudogap: friend or foe of high T_c ?, *Advances in Physics* **54**, 715 (2005), <https://doi.org/10.1080/00018730500459906>.
- [38] Y. Schattner, M. H. Gerlach, S. Trebst, and E. Berg, Competing orders in a nearly antiferromagnetic metal, *Phys. Rev. Lett.* **117**, 097002 (2016).
- [39] H. Yamase, A. Eberlein, and W. Metzner, Coexistence of incommensurate magnetism and superconductivity in the two-dimensional hubbard model, *Phys. Rev. Lett.* **116**, 096402 (2016).
- [40] Dombre, Thierry, Modulated spiral phases in doped quantum antiferromagnets, *J. Phys. France* **51**, 847 (1990).
- [41] H. J. Schulz, Incommensurate antiferromagnetism in the two-dimensional hubbard model, *Phys. Rev. Lett.* **64**, 1445 (1990).
- [42] B. I. Shraiman and E. D. Siggia, Excitation spectrum of the spiral state of a doped antiferromagnet, *Phys. Rev. B* **46**, 8305 (1992).
- [43] A. V. Chubukov and K. A. Musaelian, Magnetic phases of the two-dimensional hubbard model at low doping, *Phys. Rev. B* **51**, 12605 (1995).
- [44] A. V. Chubukov, S. Sachdev, and T. Senthil, Large-S expansion for quantum antiferromagnets on a triangular lattice, *Journal of Physics: Condensed Matter* **6**, 8891 (1994).
- [45] A. V. Chubukov and D. K. Morr, Electronic structure of underdoped cuprates, *Physics Reports* **288**, 355 (1997).
- [46] J. R. Schrieffer, X. G. Wen, and S. C. Zhang, Dynamic spin fluctuations and the bag mechanism of high- T_c superconductivity, *Phys. Rev. B* **39**, 11663 (1989).
- [47] A. V. Chubukov and D. M. Frenkel, Renormalized perturbation theory of magnetic instabilities in the two-dimensional hubbard model at small doping, *Phys. Rev. B* **46**, 11884 (1992).
- [48] N. D. Mermin and H. Wagner, Absence of ferromagnetism or antiferromagnetism in one- or two-dimensional isotropic heisenberg models, *Phys. Rev. Lett.* **17**, 1133 (1966).
- [49] This expression is obtained by collecting the renormalizations of the vertex function $\Gamma_{\alpha\beta,\gamma\delta}(K, P; P, K)$ ($K = (\mathbf{k}, \omega_{m,k})$) that contain polarization bubbles $\Pi(K - P)$ and neglecting all other contributions. This vertex function is different from $\Gamma^\omega(K, P; K, P)$ which determines low-energy physics of a Fermi liquid.
- [50] S. Chakravarty, B. I. Halperin, and D. R. Nelson, Two-dimensional quantum heisenberg antiferromagnet at low temperatures, *Phys. Rev. B* **39**, 2344 (1989).
- [51] P. Hasenfratz and F. Niedermayer, The exact correlation length of the antiferromagnetic d=2+1 heisenberg model at low temperatures, *Physics Letters B* **268**, 231 (1991).
- [52] A. J. Millis, Effect of a nonzero temperature on quantum critical points in itinerant fermion systems, *Phys. Rev. B* **48**, 7183 (1993).
- [53] B. I. Shraiman and E. D. Siggia, Spiral phase of a doped quantum antiferromagnet, *Phys. Rev. Lett.* **62**, 1564 (1989).
- [54] A. V. Chubukov and K. A. Musaelian, Systematic 1/S study of the two-dimensional Hubbard model at half-filling, *Phys. Rev. B* **50**, 6238 (1994).
- [55] C. Zhou and H. J. Schulz, Quantum fluctuations in the spiral phase of the hubbard model, *Phys. Rev. B* **52**, R11557 (1995).

- [56] A. Wietek, Y.-Y. He, S. R. White, A. Georges, and E. M. Stoudenmire, Stripes, antiferromagnetism, and the pseudogap in the doped hubbard model at finite temperature, *Phys. Rev. X* **11**, 031007 (2021).
- [57] D. P. Arovas, E. Berg, S. A. Kivelson, and S. Raghu, The hubbard model, *Annual Review of Condensed Matter Physics* **13**, 239 (2022), <https://doi.org/10.1146/annurev-conmatphys-031620-102024>.
- [58] D. Haug, V. Hinkov, Y. Sidis, P. Bourges, N. B. Christensen, A. Ivanov, T. Keller, C. T. Lin, and B. Keimer, Neutron scattering study of the magnetic phase diagram of underdoped $\text{YBa}_2\text{Cu}_3\text{O}_{6+x}$, *New Journal of Physics* **12**, 105006 (2010).
- [59] J. M. Tranquada, Spins, stripes, and superconductivity in hole-doped cuprates, *AIP Conference Proceedings* **1550**, 114 (2013), <https://aip.scitation.org/doi/pdf/10.1063/1.4818402>.
- [60] D. Chowdhury, A. Georges, O. Parcollet, and S. Sachdev, Sachdev-ye-kitaev models and beyond: Window into non-fermi liquids, *Rev. Mod. Phys.* **94**, 035004 (2022).

Appendix A: Path integral description

Here, we demonstrate the path integral representation for the fully renormalized fermion Green's function and spin susceptibility with *only* static magnetic fluctuations. We first review the path integral formulation in the quasi-static limit and then obtain the expressions for the two-point and four-point correlation functions. The point of departure is the effective action for the spin-fermion model,

$$\mathcal{Z} = \int \mathcal{D}[\bar{\psi}, \psi] e^{-\mathcal{S}_{sf}},$$

$$\mathcal{S}_{sf} = \int_{\tau} \int_{\tau'} \left(\sum_{\mathbf{k}, s} \bar{\psi}_{\mathbf{k}, s}(\tau) \left(-\mathcal{G}_{0, \mathbf{k}}^{-1} \psi_{\mathbf{k}, s}(\tau') \right) - 2g^2 \sum_{\mathbf{q}} \chi_{\mathbf{q}}(\tau - \tau') \hat{\vec{S}}_{\mathbf{q}}(\tau) \cdot \hat{\vec{S}}_{-\mathbf{q}}(\tau') \right), \quad (\text{A1})$$

where $\int_{\tau} = \int_0^{\beta} d\tau$, $\mathcal{G}_{0, \mathbf{k}}^{-1}(\tau - \tau') = -(\partial_{\tau} + \epsilon_{\mathbf{k}} - \mu)\delta(\tau - \tau')$, $\hat{\vec{S}}_{\mathbf{q}}(\tau) = \frac{1}{2} \sum_{\mathbf{k}} \bar{\psi}_{\mathbf{k}+\mathbf{q}, s}(\tau) \hat{\vec{\sigma}}_{s, s'} \psi_{\mathbf{k}, s'}(\tau)$. Here, ψ is the Grassmann fermionic field. For now, we define g as a phenomenological coupling constant. In the Matsubara frequency representation, the action becomes

$$\mathcal{S}_{sf} = \sum_{\mathbf{k}, \sigma, n} \bar{\psi}_{\mathbf{k}, \sigma, n} (-i\omega_n + \epsilon_{\mathbf{k}} - \mu) \psi_{\mathbf{k}, \sigma, n} - 2g^2 \beta^{-1} \sum_{\mathbf{q}, m} \chi_{\mathbf{q}}(\Omega_m) \hat{\vec{S}}_{\mathbf{q}}(\Omega_m) \cdot \hat{\vec{S}}_{-\mathbf{q}}(-\Omega_m) \quad (\text{A2})$$

where $\beta = 1/T$, $\psi(\tau) = \frac{1}{\sqrt{\beta}} \sum_n e^{-i\omega_n \tau} \psi_n$, $\hat{S}(\tau) = \frac{1}{\beta} \sum_m e^{i\Omega_m \tau} \hat{S}_m$, $\chi_{\mathbf{q}}(\tau - \tau') = \frac{1}{\beta} \sum_m \chi_{\mathbf{q}}(\Omega_m) e^{i\Omega_m(\tau - \tau')}$ and $\chi_{\mathbf{q}}(\Omega_m) = \frac{\chi_0}{\Omega_m^2 + v_s^2(\mathbf{q} - \mathbf{Q})^2 + v_s^2 \xi^{-2}}$.

We next insert the identity $\int \mathcal{D}[\vec{S}] e^{-\frac{\beta}{2} \sum_{\mathbf{q}} \chi_{\mathbf{q}}^{-1}(\Omega_m) \vec{S}_{\mathbf{q}, m} \vec{S}_{-\mathbf{q}, -m}} = 1$, and through the Hubbard-Stratonovich transformation, the partition function becomes

$$\mathcal{Z} = \int \mathcal{D}[\bar{\psi}, \psi, \vec{S}] e^{-\mathcal{S}_{sf}}$$

$$\mathcal{S}_{sf} = \sum_{\mathbf{k}, s, n, \mathbf{k}', s', n'} \bar{\psi}_{\mathbf{k}, s, n} \left(-(i\omega_n - \epsilon_{\mathbf{k}} + \mu) \delta_{\mathbf{k}\mathbf{k}'} \delta_{ss'} \delta_{nn'} - g \vec{S}_{\mathbf{q}, m} \cdot \frac{\vec{\sigma}_{ss'}}{2} \delta_{\mathbf{k}+\mathbf{q}, \mathbf{k}'} \delta_{m+n, n'} \right) \psi_{\mathbf{k}', s', n'}$$

$$+ \frac{\beta}{2} \sum_{\mathbf{q}, m} \chi_{\mathbf{q}}^{-1}(\Omega_m) \vec{S}_{\mathbf{q}, m} \cdot \vec{S}_{-\mathbf{q}, -m} \quad (\text{A3})$$

Note that no approximation is made to obtain Eq. (A3), but it cannot be solved exactly in general.

To consider *only* the static spin fluctuations, we restrict to the zero Matsubara frequency for the spin field \vec{S} ; the partition function becomes

$$\mathcal{Z} = \int \mathcal{D}[\bar{\psi}, \psi, \vec{S}] e^{-\mathcal{S}_{\text{static}}}$$

$$\mathcal{S}_{\text{static}} = \sum_{\mathbf{k}, s, n, \mathbf{k}', s'} \bar{\psi}_{\mathbf{k}, s, n} \left(-(i\omega_n - \epsilon_{\mathbf{k}} + \mu) \delta_{\mathbf{k}\mathbf{k}'} \delta_{ss'} - 2g \vec{S}_{\mathbf{q}} \cdot \frac{\vec{\sigma}_{ss'}}{2} \delta_{\mathbf{k}+\mathbf{q}, \mathbf{k}'} \right) \psi_{\mathbf{k}', s', n} + \frac{\beta}{2} \sum_{\mathbf{q}} \chi_{\mathbf{q}}^{-1} \vec{S}_{\mathbf{q}} \cdot \vec{S}_{-\mathbf{q}}. \quad (\text{A4})$$

Here, we have replaced $\vec{S}_{\mathbf{q}}$ with $\vec{S}_{\mathbf{q}, 0}$ for convenience, and $\chi_{\mathbf{q}}^{-1} = (v_s^2(\mathbf{q} - \mathbf{Q})^2 + v_s^2 \xi^{-2})/\chi_0$ is the static spin susceptibility. Eq. (A4) may be viewed as an annealed disorder problem, with $\vec{S}_{\mathbf{q}}$ as the static spin impurity. Integrating out the fermion field ψ , we get the effective action in terms of only the spin fields

$$\mathcal{Z} = \int \mathcal{D}[\vec{S}] \exp \left(\text{tr} \ln \mathcal{M}(\vec{S}) - \frac{\beta}{2} \sum_{\mathbf{q}} \chi_{\mathbf{q}}^{-1} \vec{S}_{\mathbf{q}} \cdot \vec{S}_{-\mathbf{q}} \right) \quad (\text{A5})$$

$[\mathcal{M}(\vec{S})]_{\mathbf{k}s, \mathbf{k}'s'} = \left((i\omega_n - \epsilon_{\mathbf{k}} + \mu) \delta_{\mathbf{k}\mathbf{k}'} \delta_{ss'} + g \vec{S}_{\mathbf{k}'-\mathbf{k}} \cdot \vec{\sigma}_{ss'} \right)$ is the inverse Green's function in a particular spin configu-

ration determined by $\vec{S}_{\mathbf{k}'-\mathbf{k}}$. To compute the n-point correlation function, we define the generating functional as

$$\mathcal{W}(\bar{\eta}, \eta) = \int \mathcal{D} [\bar{\psi}, \psi, \vec{S}] \exp(-(\bar{\psi}\eta + \bar{\eta}\psi + \mathcal{S}_{\text{static}})), \quad (\text{A6})$$

with the shorthand notation $\bar{\psi}\eta = \sum_{\mathbf{k}, s, n} \bar{\psi}_{\mathbf{k}, s, n} \eta_{\mathbf{k}, s, n}$.

The full Green's function, i.e. the two-point correlation function, reads

$$\begin{aligned} G(i\omega_n, \mathbf{k}, \mathbf{k}')_{ss'} &= \langle G(i\omega_n, \mathbf{k}, \mathbf{k}') | \vec{S} \rangle_{ss'} |_{\vec{S}} = \frac{1}{\mathcal{Z}} \frac{\partial^2 \mathcal{W}(\eta, \bar{\eta})}{\partial \bar{\eta}_s \partial \eta_{s'}} \Big|_{\eta, \bar{\eta}=0} \\ &= \frac{\int \mathcal{D} [\vec{S}] [\mathcal{M}(\vec{S})^{-1}]_{\mathbf{k}s, \mathbf{k}'s'} \exp\left(\text{tr} \ln \mathcal{M}(\vec{S}) - \frac{\beta}{2} \sum_{\mathbf{q}} \chi_{\mathbf{q}}^{-1} \vec{S}_{\mathbf{q}} \cdot \vec{S}_{-\mathbf{q}}\right)}{\int \mathcal{D} [\vec{S}] \exp\left(\text{tr} \ln \mathcal{M}(\vec{S}) - \frac{\beta}{2} \sum_{\mathbf{q}} \chi_{\mathbf{q}}^{-1} \vec{S}_{\mathbf{q}} \cdot \vec{S}_{-\mathbf{q}}\right)} \\ &\approx \frac{\int \mathcal{D} [\vec{S}] [\mathcal{M}(\vec{S})^{-1}]_{\mathbf{k}s, \mathbf{k}'s'} \exp\left(-\frac{\beta}{2} \sum_{\mathbf{q}} \tilde{\chi}_{\mathbf{q}}^{-1} \vec{S}_{\mathbf{q}} \cdot \vec{S}_{-\mathbf{q}}\right)}{\int \mathcal{D} [\vec{S}] \exp\left(-\frac{\beta}{2} \sum_{\mathbf{q}} \tilde{\chi}_{\mathbf{q}}^{-1} \vec{S}_{\mathbf{q}} \cdot \vec{S}_{-\mathbf{q}}\right)} \end{aligned} \quad (\text{A7})$$

From the second to the third line, we assume that the feedback effects on \vec{S} from the fermions, written as $\text{tr} \ln \mathcal{M}(\vec{S})$, can be fully captured by replacing the spin susceptibility χ with a renormalized one $\tilde{\chi}$, which is determined independently from the four-point correlation function.

The static spin polarization $\Pi^{\alpha\beta}(\mathbf{q})$ can be expressed as the four-point correlation function

$$\begin{aligned} \Pi^{\alpha\beta}(\mathbf{q}) &= \langle \Pi^{\alpha\beta}(\mathbf{q} | \vec{S}) \rangle_{\vec{S}} = \frac{1}{\mathcal{Z}} \frac{\partial^4 \mathcal{W}(\eta, \bar{\eta})}{\partial \bar{\eta} \partial \eta \partial \bar{\eta} \partial \eta} \Big|_{\eta, \bar{\eta}=0} \\ &\approx \frac{\int \mathcal{D} [\vec{S}] \text{tr} \left[-\frac{1}{2} \sigma^\alpha [\mathcal{M}(\vec{S})^{-1}]_{\mathbf{k}+\mathbf{q}, \mathbf{k}'\sigma^\beta} [\mathcal{M}(\vec{S})^{-1}]_{\mathbf{k}'-\mathbf{q}, \mathbf{k}} \right] \exp\left(-\frac{\beta}{2} \sum_{\mathbf{q}} \tilde{\chi}_{\mathbf{q}}^{-1} \vec{S}_{\mathbf{q}} \cdot \vec{S}_{-\mathbf{q}}\right)}{\int \mathcal{D} [\vec{S}] \exp\left(-\frac{\beta}{2} \sum_{\mathbf{q}} \tilde{\chi}_{\mathbf{q}}^{-1} \vec{S}_{\mathbf{q}} \cdot \vec{S}_{-\mathbf{q}}\right)}, \end{aligned} \quad (\text{A8})$$

where the spin index in $\eta, \bar{\eta}$ is omitted.

To determine $\tilde{\chi}_{\mathbf{q}}$, we note that it is related to the irreducible particle-hole polarization $\Pi^{\alpha\beta}(\mathbf{q})$ as

$$\tilde{\chi}_{\mathbf{q}} = \frac{\Pi^{\alpha\alpha}(\mathbf{q})/2}{1 - U\Pi^{\alpha\alpha}(\mathbf{q})} \quad (\text{A9})$$

where we have used the fact that due to the SU(2) symmetry in the paramagnetic state, the static spin polarization is diagonal, i.e. $\Pi^{\alpha, \beta \neq \alpha}(\mathbf{q}) = 0$. Assuming that $\chi_{\mathbf{q}}$ takes the standard Ornstein-Zernike form near $\mathbf{q} \approx \mathbf{Q}$, i.e. $\tilde{\chi}_{\mathbf{q}} = \chi_0 / (v_s^2(\mathbf{q} - \mathbf{Q})^2 + v_s^2 \xi^{-2})$, the spin correlation length ξ in $\tilde{\chi}_{\mathbf{q}}$ reads

$$\xi^{-2} = \frac{\chi_0}{v_s^2} \frac{1 - U\Pi^{zz}(\mathbf{Q})}{\Pi^{zz}(\mathbf{Q})} \approx \frac{2U\chi_0}{v_s^2} (1 - U\Pi^{zz}(\mathbf{Q})) \quad (\text{A10})$$

Plugging (A8) into (A10), we can solve for ξ self-consistently. To simplify the evaluation, it is convenient to integrate out the spin fields \vec{S} and obtain a compact form for (A7) and (A8). Here, following the suggestion from the one-loop calculation as demonstrated in Sec. III C, we ignore the spacial fluctuations of the fermion fields. This allows us to replace $\vec{S}_{\mathbf{q}}$ with $\vec{S}_{\mathbf{Q}}$ in the fermion propagator, i.e.

$$[\mathcal{M}(\vec{S})]_{\mathbf{k}s, \mathbf{k}'s'} \approx \left((i\omega_n - \epsilon_{\mathbf{k}}) \delta_{\mathbf{k}\mathbf{k}'} \delta_{ss'} + g\beta^{-1} \vec{S}_{\mathbf{Q}} \cdot \vec{\sigma}_{ss'} \delta_{\mathbf{k}+\mathbf{Q}, \mathbf{k}'} \right). \quad (\text{A11})$$

Including only the spatial fluctuations for the spin fields, we have

$$\exp\left(-\frac{1}{2\beta} \sum_{\mathbf{q}} \tilde{\chi}_{\mathbf{q}}^{-1} \vec{S}_{\mathbf{q}} \cdot \vec{S}_{-\mathbf{q}}\right) \approx \exp\left(-\frac{1}{2\beta} \left(\sum_{\mathbf{q}} \tilde{\chi}_{\mathbf{q}}\right)^{-1} \vec{S}_{\mathbf{Q}} \cdot \vec{S}_{-\mathbf{Q}}\right) = \exp\left(-4t^{-1} \vec{S}_{\mathbf{Q}} \cdot \vec{S}_{\mathbf{Q}}\right), \quad (\text{A12})$$

where we remind $\mathbb{t} = \frac{4T}{\pi J} \ln \frac{\pi^2/2 + \xi^{-2}}{\epsilon^2 + \xi^{-2}}$. To obtain the last line, we have rescaled $\vec{S}_{\mathbf{Q}}$ as $\beta^{-1} \vec{S}_{\mathbf{Q}} \Rightarrow \vec{S}_{\mathbf{Q}}$, and will use this definition hereafter. Using Eqs. (A11) and (A12), the two- and four-point correlation functions are approximated as

$$G(i\omega_n, \mathbf{k}, \mathbf{k}')_{ss'} = \langle G(i\omega_n, \mathbf{k}, \mathbf{k}') | \vec{S} \rangle_{\vec{S}} \approx \frac{\int d\vec{S}_{\mathbf{Q}} [\mathcal{M}(\vec{S})^{-1}]_{\mathbf{k}s, \mathbf{k}'s'} \exp(-4\mathbb{t}^{-1} \vec{S}_{\mathbf{Q}} \cdot \vec{S}_{\mathbf{Q}})}{\int d\vec{S}_{\mathbf{Q}} \exp(-4\mathbb{t}^{-1} \vec{S}_{\mathbf{Q}} \cdot \vec{S}_{\mathbf{Q}})}$$

$$\Pi^{\alpha\beta}(\mathbf{q}) = \langle \Pi^{\alpha\beta}(\mathbf{q} | \vec{S}) \rangle_{\vec{S}} \approx -\frac{1}{2} \frac{\int d\vec{S}_{\mathbf{Q}} \sum_{s_i} \sigma_{s_1 s_2}^{\alpha} [\mathcal{M}(\vec{S})^{-1}]_{\mathbf{k}+\mathbf{Q}s_2, \mathbf{k}'s_3} \sigma_{s_3 s_4}^{\beta} [\mathcal{M}(\vec{S})^{-1}]_{\mathbf{k}'-\mathbf{Q}s_4, \mathbf{k}s_1} \exp(-4\mathbb{t}^{-1} \vec{S}_{\mathbf{Q}} \cdot \vec{S}_{\mathbf{Q}})}{\int d\vec{S}_{\mathbf{Q}} \exp(-4\mathbb{t}^{-1} \vec{S}_{\mathbf{Q}} \cdot \vec{S}_{\mathbf{Q}})} \quad (\text{A13})$$

where

$$[\mathcal{M}(\vec{S})^{-1}]_{\mathbf{k}, \mathbf{k}'} = \frac{1}{1 - g^2/4 \vec{S}_{\mathbf{Q}} \cdot \vec{S}_{\mathbf{Q}} \mathcal{H}_{\mathbf{k}, n}} \begin{pmatrix} G^{(0)}(\mathbf{k}, i\omega_n) \mathbb{1}_{\sigma} \delta_{\mathbf{k}, \mathbf{k}'} & -\frac{g}{2} \vec{S}_{\mathbf{Q}} \cdot \vec{\sigma} \mathcal{H}_{\mathbf{k}, n} \delta_{\mathbf{k}+\mathbf{Q}, \mathbf{k}'} \\ -\frac{g}{2} \vec{S}_{\mathbf{Q}} \cdot \vec{\sigma} \mathcal{H}_{\mathbf{k}, n} \delta_{\mathbf{k}, \mathbf{k}'+\mathbf{Q}} & G^{(0)}(\mathbf{k} + \mathbf{Q}, i\omega_n) \mathbb{1}_{\sigma} \delta_{\mathbf{k}+\mathbf{Q}, \mathbf{k}'+\mathbf{Q}} \end{pmatrix} \quad (\text{A14})$$

with $\mathcal{H}_{\mathbf{k}, n} = G^{(0)}(\mathbf{k}, i\omega_n) G^{(0)}(\mathbf{k} + \mathbf{Q}, i\omega_n)$.

Below and close to T_N , we restrict the spin fluctuations to the transverse channel, i.e. $\vec{S}_{\mathbf{Q}} = (S_x, S_y, \langle S_z \rangle) = (S_x, S_y, \Delta/U)$, and only S_x, S_y are the static fluctuating fields. Now, we identify the coupling $g/2$ with the Hubbard interaction U . Eq. (A13) becomes

$$G(i\omega_n, \mathbf{k}, \mathbf{k})_{ss} = \frac{G^{(0)}(\mathbf{k}, i\omega_n)}{1 - \Delta^2 \mathcal{H}_{\mathbf{k}, n}} \int_0^{\infty} \frac{1}{1 - u_{\omega} t} \exp(-t)$$

$$G(i\omega_n; \mathbf{k}, \mathbf{k} + \mathbf{Q})_{ss} = \text{sgn } s \frac{-\Delta \mathcal{H}_{\mathbf{k}, \omega}}{1 - \Delta^2 \mathcal{H}_{\mathbf{k}, n}} \int_0^{\infty} \frac{1}{1 - u_{\omega} t} \exp(-t)$$

$$\Pi^{zz}(\mathbf{q}) \stackrel{T > T_N}{=} \frac{-4}{\mathbb{t}} T \sum_{n, \mathbf{k}} \int dS_x dS_y \frac{2\mathcal{H}_{\mathbf{k}}}{1 - U^2(S_x^2 + S_y^2) \mathcal{H}_{\mathbf{k}, n}} \exp(-4\mathbb{t}^{-1}(S_x^2 + S_y^2))$$

$$= -\frac{1}{\mathbb{t}(U/2)^2} \int \frac{d\omega}{\pi} n_F(\omega) \text{Im} \left[\int_0^{\infty} dt \frac{1}{t - u_{\omega}^{-1}} \exp(-t) \right]$$

$$= -\frac{1}{\mathbb{t}(U/2)^2} \int d\omega n_F(\omega) \text{sgn}(\bar{\omega}) \Theta(\bar{\omega} - (\varepsilon_{\mathbf{k}}^-)^2) \exp\left(-\frac{\bar{\omega}^2 - (\varepsilon_{\mathbf{k}}^-)^2}{\mathbb{t}(U/2)^2}\right) \quad (\text{A15})$$

where $u_{\omega} = \frac{(U/2)^2 \mathcal{H}_{\mathbf{k}, \omega}}{1 - \Delta^2 \mathcal{H}_{\mathbf{k}, \omega}}$, $n_F(\omega) = (\exp(\omega) + 1)^{-1}$, $\bar{\omega} = \omega + \mu - \varepsilon_{\mathbf{k}}^+$, $E_{\mathbf{k}}^2 = (\varepsilon_{\mathbf{k}}^-)^2 + \Delta^2$. At $T > T_N$, $\Delta = 0$.